Glucosylceramide synthesis inhibition affects cell cycle progression, membrane trafficking, and stage differentiation in Giardia lamblia

Štefanić, Saša ; Spycher, C ; Morf, L ; Fabriàs, G ; Casas, J ; Schraner, E ; Wild, P ; Hehl, A B ; Sonda, S

Abstract: Synthesis of glucosylceramide via glucosylceramide synthase (GCS) is a crucial event in higher eukaryotes, both for the production of complex glycosphingolipids and for regulating cellular levels of ceramide, a potent antiproliferative second messenger. In this study, we explored the dependence of the early branching eukaryote Giardia lamblia on GCS activity. Biochemical analyses revealed that the parasite has a GCS located in endoplasmic reticulum (ER) membranes that is active in proliferating and encysting trophozoites. Pharmacological inhibition of GCS induced aberrant cell division, characterized by arrest of cytokinesis, incomplete cleavage furrow formation, and consequent block of replication. Importantly, we showed that increased ceramide levels were responsible for the cytokinesis arrest. In addition, GCS inhibition resulted in prominent ultrastructural abnormalities, including accumulation of cytosolic vesicles, enlarged lysosomes, and clathrin disorganization. Moreover, anterograde trafficking of the encystations-specific protein CWP1 was severely compromised and resulted in inhibition of stage differentiation. Our results reveal novel aspects of lipid metabolism in G. lamblia and specifically highlight the vital role of GCS in regulating cell cycle progression, membrane trafficking events, and stage differentiation in this parasite. In addition, we identified ceramide as a potent bioactive molecule, underscoring the universal conservation of ceramide signaling in eukaryotes.

DOI: https://doi.org/10.1194/jlr.M003392

Inhibition of glucosylceramide synthesis affects cell cycle progression, membrane trafficking and stage differentiation in the minimized protozoan *Giardia lamblia.*

Saša Štefanić[1†], Cornelia Spycher[1], Laura Morf[1], Gemma Fabriàs[2], Josefina Casas[2], Elisabeth Schraner[3], Peter Wild[3], Adrian B. Hehl[1]* and Sabrina Sonda[1]*

[1]Institute of Parasitology and [3]Institute of Veterinary Anatomy, University of Zurich, 8057 Zurich, Switzerland; [2] Institut de Química Avançada de Catalunya, Consejo Superior de Investigaciones Científicas (CSIC), 08034 Barcelona, Spain.

†Present address: Sandler Center for Basic Research in Parasitic Diseases, QB3, Byers Hall 508-B, Mission Bay Campus, University of California San Francisco, San Francisco, CA 94158-2550, USA.

Running title: Inhibition of glucosylceramide synthesis in *G. lamblia*.

*Address correspondence to:

Sabrina Sonda, sabrina.sonda@vetparas.uzh.ch. Tel. +41 44 635 85 14. FAX +41 44 635 89 07

Adrian B. Hehl, adrian.hehl@access.uzh.ch. Tel. +41 44 635 85 26. FAX +41 44 635 89 07

Institute of Parasitology, University of Zurich. Winterthurerstrasse 266a , 8057 Zurich, Switzerland.

Abbreviations: PPMP, DL-*threo*-1-Phenyl-2-palmitoylamino-3-morpholino-1-propanol; PVs, peripheral vesicles; ESVs, encystation-specific vesicles; CWP, cyst wall protein, GCS, glucosylceramide synthase; CTX, cholera toxin B subunit; ER, endoplasmic reticulum.

Abstract

Synthesis of glucosylceramide via glucosylceramide synthase (GCS) is a crucial event in higher eukaryotes, both for the production of complex glycosphingolipids and for regulating cellular levels of ceramide, a potent anti-proliferative second messenger. In this study, we explored the dependence of the early branching eukaryote *Giardia lamblia* on GCS activity. Biochemical analyses revealed that the parasite has a GCS located in ER membranes that is active in proliferating and encysting trophozoites. Pharmacological inhibition of GCS induced aberrant cell division, characterized by arrest of cytokinesis, incomplete cleavage furrow formation and consequent block of replication. Importantly, we showed that increased ceramide levels were responsible for the cytokinesis arrest. In addition, GCS inhibition resulted in prominent ultrastructural abnormalities, including accumulation of cytosolic vesicles, enlarged lysosomes and clathrin disorganization. Moreover, anterograde trafficking of the encystation specific protein CWP1 was severely compromised and resulted in inhibition of stage differentiation. Our results reveal novel aspects of lipid metabolism in *G. lamblia* and specifically highlight the vital role of GCS in regulating cell cycle progression, membrane trafficking events and stage differentiation in this parasite. In addition, we identified ceramide as a potent bioactive molecule, underscoring the universal conservation of ceramide signaling in eukaryotes.

Supplementary key words: Glucosylceramide, ceramide, *Giardia lamblia*, cell division, vesicular trafficking, differentitation.

Introduction

Sphingolipids are a highly complex class of lipids in terms of structural diversity, metabolism and cellular functions. While initially seen as inert structural components of eukaryotic cell membranes, there is now substantial evidence that sphingolipids play an important role in signal transduction (for a recent review on bioactive sphingolipids see [1]).

Ceramide, a central molecule in the sphingolipid biosynthesis, plays a critical role as second messenger in cellular signaling which regulates anti-proliferative processes, including apoptosis, cell differentiation, and cell cycle arrest in different cell types. Being a highly bioactive molecule, ceramide levels must be tightly controlled by diverse coordinated mechanisms, including ceramide degradation, phosphorylation or sphingolipid metabolism. Glucosylceramide synthase (GCS), also defined as ceramide glucosyltransferase (CGT), metabolizes ceramide to glucosylceramide (GlcCer), a glycosylated form of ceramide that does not have anti-proliferative activity. GCS plays a crucial role in cell survival after apoptotic stimuli, as demonstrated by the up-regulation of GCS and GlcCer in some multidrug resistant tumor cells to counteract a chemotherapy-induced increase of ceramide [2, 3]. Conversely, decreased GCS activity by RNA interference or by pharmacological inhibition of GCS activity with PPMP (DL-*threo*-1-Phenyl-2-palmitoylamino-3-morpholino-1-propanol) leads to ceramide buildup and cytotoxicity [4, 5]. Thus, GCS is considered a pivotal regulator of bioactive ceramide levels.

Sphingolipid metabolism in pathogenic protozoa is the object of increasing interest as a source of promising chemotherapy targets. We recently showed that PPMP has a potent inhibitory effect on *Giardia lamblia* [6], a protozoan parasite which has undergone massive minimization during evolution [7], and is a leading cause of intestinal infection worldwide [8]. Both stages of the parasite's life cycle, namely replicating trophozoites, responsible for pathogenesis, and

environmentally resistant cysts, responsible for disease transmission, were affected by PPMP at concentrations that are not toxic for mammalian cells. The observed sensitivity to PPMP suggested that an active GCS may exist in the parasite; in addition, a GCS homologue, GL50803_11642, is annotated in the *G. lamblia* Genome Database (http://giardiadb.org) and its transcription has been reported to be regulated during the parasite's life cycle [9]. Moreover, the predicted ORF GL50803_7598 contains a domain typical of the glycolipid transfer protein (GLTP) superfamily. While the precise cellular function of GLTP remains undefined, a proposed correlation between presence of a GLTP and GCS activity [10] further supports the presence of an active GCS in the parasite.

However, the synthesis of sphingolipids and of GlcCer in particular has not been demonstrated in the parasite so far. Lipid neosynthesis is limited in *G. lamblia*, and the parasite is thought to rely on lipids taken up from the environment, namely the host intestinal content. Indeed, *in vitro* analyses showed negligible incorporation of lipid precursors, such as acetate and glycerol [11], while robust incorporation of exogenous radiolabeled fatty acids [12-14], phospholipids [14] ceramide and gangliosides [15, 16] could be demonstrated. In addition, uptake of fluorescent sphingolipid analogues, including ceramide and sphingomyelin, has been reported [12, 14, 15]. Importantly, acyl chain desaturation [17], deacylation/reacylation and head group exchange [18] have been shown to occur in *G. lamblia*, indicating that the parasite can remodel the incorporated exogenous lipids to fulfill its own needs.

In this study, we used a biochemical approach to address whether the synthesis of GlcCer occurs in *G. lamblia* and whether it can be inhibited by PPMP. In addition, we investigated the molecular mechanism of PPMP-mediated effects in more detail and identified ceramide as a key modulator of cellular processes in this parasite.

Materials and methods

Biochemical reagents. Unless otherwise stated, all chemicals were purchased from Sigma and cell culture reagents from Gibco-BRL. Inhibitor stock solutions were prepared at the following concentrations: 10 mM DL-*threo*-1-Phenyl-2-palmitoylamino-3-morpholino-1-propanol (PPMP), 14 mM fumonisin B1 (FB1), 5 mM myriocin (Myr), 250 mM L-cycloserine (L-cyc), 22.5 mM N-butyldeoxynojirimycin (NB-DNJ), 3 mM tunicamycin (TM), 16.6 mM nocodazole and 20 mg/mL puromycin. Inhibitors were freshly diluted to the concentrations required for the individual experiment.

Parasite cell culture. Trophozoites of the *Giardia lamblia* strain WBC6 (ATCC catalog number 50803) were grown axenically as described [6]. Harvested parasites were counted using the improved Neubauer chamber. New subcultures were obtained by inoculating $5x10^4$ trophozoites from confluent cultures into new 11 mL culture tubes.

Two-step encystation was induced as described previously [19, 20], by cultivating the cells for ~44 h in medium without bile (pre-encysting medium) and subsequently in medium with higher pH and porcine bile (encysting medium).

Drug treatment of trophozoites was performed on freshly inoculated subcultures. Parasites were allowed to adhere for 8 h and then incubated for additional 16 h with the inhibitors at the concentrations indicated in the figure legend of the individual experiments. Drug treatment of encysting cells was performed in two steps: 7 h drug incubation in pre-encysting medium and additional 16 h incubation in encysting medium. For replication and doublet formation assay, cells were harvested and counted as described above.

For reversibility assay, freshly inoculated subcultures were incubated with the inhibitor for 16 h as described above, harvested and washed to remove the drug. Collected parasites were then counted and re-inoculated in absence of inhibitor for additional 4 days, followed by counting.

Expression vector construction and transfection. All constructs of giardial glucosylceramide synthase (GCS) (GL50803_11642) were based on the expression cassette C1-CWP for inducible expression under the control of the CWP1 promoter [19]. For N-terminal tagging with the hemagglutinin (HA) epitope, full length GCS (aa 2 – 537) and variant without putative signal peptide (aa 23 – 537) coding regions were amplified by PCR and cloned in a vector containing the HA epitope tag upstream of the NsiI restriction site. For C-terminal tagging, the HA epitope tag was encoded on the antisense primer and the product cloned into an identical vector variant devoid of N-terminal HA-tag. Because giardial GCS coding sequence contains an NsiI restriction site, a complementary SbfI restriction site was encoded on sense primers and used for ligation into the vectors.

Stable chromosomal integration of the described constructs was performed using the pPacV-Integ expression vector [21] using *XbaI* and *Pac*I restriction sites. Oligonucleotides (5'-3' orientation) used in this study were:

GCS(2-537)-*SbfI*-s AGATCTCCTGCAGGACGGGTTGACTCTCTCCTTAGTG; GCS (23-537)-*SbfI*-s AGATCTCCTGCAGGCTGTCAACCGCATAAGTG; GCS-*PacI*-as CGTTAATT AATCAGTCGAGGGATTTTTTATTGGCCTG;GCS-HA-*PacI*-asCGTTAATTAATCACGCGT AGTCTGGGACATCGTATGGGTAGTCGAGGGATTTTTTATTGGCCTG.

Plasmid vector DNA was linearized using *SwaI* restriction enzyme and 15 µg of digested plasmid DNA was electroporated (350V, 960µF, 800Ω) into trophozoites. Linearized plasmid

targets the *G. lamblia* triose phosphate isomerase locus (GL50803_93938) and integration occurs by homologous recombination under selective pressure with the antibiotic puromycin [22].

Gene expression analysis. RNA was isolated from trophozoites or parasites allowed to encyst for 7 h using an RNAeasy kit (Qiagen, Stanford, CA) following the "Animal Cells Spin" protocol. Residual genomic DNA was removed with DNase 1 digestion according to the manufacturer's protocol. The integrity of the RNA was analyzed in a Bioanalyser (Agilent Technologies Inc., Palo Alto, CA) with "Eukaryote Total RNA Nano Series II" settings.

For dual channel microarray analysis, extracted total RNA was processed using the "Amino Allyl MessageAmp™II a RNA Amplification Kit"(Ambion, Austin, TX) and labelled with N-hydroxysuccinimidyl ester-derivatized reactive dyes Cy™3 or Cy™5, according to the manufacturer's protocol. After purification, 2 µg each of Cy3 or Cy5 labelled aRNA were denatured, added to SlideHyb™ Buffer I (Ambion), and hybridized to *G. lamblia* microarrays version 1 (TIGR) in a Tecan HybStation at the Functional Genomics Centre Zurich, Switzerland. The arrays are epoxy surface coated glass slides with ss-oligo (70 mers) containing 19230 elements and covering the whole *G. lamblia* WBC6 strain genome.

Prior hybridization, slides were hydrated and blocked with 150 µl Tris-HCl-ethanolamine (0.1 M Tris, 50 mM ethanolamine, pH 9.0), for 30 minutes at 50°C. After washing, samples were injected and hybridized for 16 h at 42°C. Slides were scanned in an Agilent Scanner G2565AA, using laser lines 543 nm and 633 nm for excitation of Cy3 and Cy5, respectively**.** Spatial scanning resolution was 10 µm, single pass. The scanner output files were quantified using the Genespotter Software (MicroDiscovery GmbH, Berlin, Germany) with default settings and 2.5 µm radius. The median spot intensities were evaluated with the Web application MAGMA [23] and normalized using the print-tip-wise loess correction of the *limma* package [24]. Potential

gene-specific dye-effects were estimated from self-self hybridizations. Differential expression of genes during encystation is reported as encystation-induced fold-change, as well as the p-value for differential expression as estimated by the empirical Bayes model implemented in *limma*. Experiments were performed in biological triplicate.

For semi-quantitative real time PCR (RT-PCR), first strand cDNA synthesis was performed using ~350 ng RNA and Omniscript reverse transcriptase (Qiagen), according to manufacturer's protocol. Amplification was performed in an iCycler iQ (Biorad, Hercules, CA) using 2 µl of 1:1000 diluted cDNA. To monitor possible contamination with residual genomic DNA, PCR amplification was performed on the extracted RNA and water. Primer pairs (5'-3' orientation) used for amplification of actin (ACT), cyst wall protein 1 (CWP1) and glucosylceramide synthetase (GCS) were: ACT-s, ACATATGAGCTGCCAGATGG; ACT-as,TCGGGGAGGCCT GCAAAC; CWP1s,GGCGATATTCCCGAGTGCATGTG; CWP1as,GTGAGGCAGTACTCTA GT; GCS-s, GCAGACCAAGCCTAGCATC; GCS-as, CCTTTACCACAGGCACTTTG. All reactions were run in triplicate. To assess the efficiency of the amplification reactions, standard curves for every primer pair and cDNA were generated from six-fold serial dilutions in duplicate, using the iQ5 software. Expression levels of the genes were given as values in arbitrary units relative to the amount of the constitutively expressed house-keeping gene actin.

Lipid analysis. For analysis of lipid synthesis in *G. lamblia* in presence of inhibitors, isolated parasites were pre-treated with the selected compounds for 30 min at 37ºC followed by labeling with 4 µCi/mL [^{3}H]palmitic acid or [^{3}H]serine for 3 h at 37ºC in supplemented PBS (PBS containing 50 mM glucose, 9 mM L-cysteine, 1.7 mM ascorbic acid, pH 7.1) in presence of the compounds. Labeling with 20 µCi/mL [^{3}H]glucose was performed in supplemented PBS without glucose addition. After extensive washing with PBS and 0.05% fat free BSA in PBS, lipids were

extracted according to [25]. When required, extracted lipids were saponified by mild alkaline hydrolysis. Lipid aliquots were separated by high performance thin layer chromatography (HPTLC) on Silica Gel 60 plates. Solvent systems used were the following: A, first dimension, chloroform:methanol:25% ammonium hydroxide:water (65:35:4:4); second dimension, chloroform:aceton:methanol:acetic acid:water (50:20:10:10:5); B, chloroform:methanol:25% ammonium hydroxide (65:25:4.5); C, chloroform:methanol:acetic acid:water (84:4.5:5:0.5) D, benzene/2-propanol/water (100:10:0.25). Radiolabeled bands were visualized using a tritium-sensitive screen (Perkin-Elmer, Boston, USA) in a Personal Molecular PhosphoImager FX (Biorad), identified according to co-migrating standards (Avanti Polar Lipids, Alabaster, USA) visualized by iodine vapors and quantified using ImageQuant software (Amersham, Otelfingen, Switzerland).

For ceramide glycanase digestion, samples were dissolved in 50 mM sodium acetate buffer pH 5.0 containing 0.1% (w/v) sodium cholate. Ceramide glycanase (Calbiochem) was added at 3.1U/mL and digestion was performed at 37^{o}C for 24 h. Lipids were extracted and analyzed by TLC.

For radioactivity incorporation analysis, parasites were labeled with radioactive precursors as described. Cell aliquots were solubilized with 0.1N NaOH or processed for lipid extraction; whole cell or lipid associated radioactivity was measured by liquid scintillation and normalized by protein content.

Liquid chromatography-mass spectrometry (LC-MS) was carried out using lipids from *G. lamblia* trophozoites, with or without PPMP treatment, and 24 h encysted cells containing an average of 33% cysts, as described [26]. Briefly, cells were harvested, washed in PBS, and transferred to glass vials. Sphingolipid extracts, fortified with internal standards (N-

dodecanoylsphingosine, N-dodecanoylglucosylsphingosine, and N-dodecanoylsphingosylphosphorylcholine, 0.5 nmol each), were prepared as described [27] and analysed. The liquid chromatography-mass spectrometer consisted of a Waters Aquity UPLC system connected to a Waters LCT Premier orthogonal accelerated time of flight mass spectrometer (Waters, Millford, MA), operated in positive electrospray ionisation mode. Full scan spectra from 50 to 1500 Da were acquired and individual spectra were summed to produce data points each 0.2 s. Mass accuracy and reproducibility were maintained by using an independent reference spray by the LockSpray interference. The analytical column was a 100 mm x 2.1 mm i.d., 1.7 µm C8 Acquity UPLC BEH (Waters). The two mobile phases were A: methanol:water:formic acid (74:25:1); B: methanol:formic acid (99:1), both also contained 5 mM ammonium formate. A linear gradient was programmed—0.0 min: 80% B; 3 min: 90% B; 6 min: 90% B; 15 min: 99% B; 18 min: 99% B; 20 min: 80% B. The flow rate was 0.3 $mLmin^{-1}$. The column was held at 30ºC. Quantification was carried out using the extracted ion chromatogram of each compound, using 50 mDa windows. The linear dynamic range was determined by injecting standard mixtures. Positive identification of compounds was based on the accurate mass measurement with an error <5 ppm and its LC retention time, compared to that of a standard (±2 %).

Fluorescence microscopy analysis. Lysotracker Blue-White (Molecular Probes) staining of live trophozoites was performed at 100 nM in supplemented PBS at 37°C for 1 hr. Cells were then resuspended in PBS and directly imaged.

For surface labeling, parasites were incubated with 6 µg/mL fluorescein-conjugated cholera toxin B subunit (Molecular Probes) in supplemented PBS for 60 min at 4°C and analyzed after fixation in 3% formaldehyde solution in PBS for 45 min on glass slides.

For membrane endocytosis, parasite were incubated with cholera toxin for 30 min at 4°C, washed in PBS, incubated at 37°C for the time indicated in the Figure legends and imaged after fixation. Endocytosis was quantified by counting the percentage of cells stained in the endocytosis signature area at the centre of the ventral disk.

For immunolabeling, cells were harvested as described above, washed twice in ice-cold PBS, and fixed as before on glass slides. Fixed cells were permeabilized with 0.2% Triton X-100 in PBS for 20 min, blocked and incubated with primary antibodies for 1 h. The primary antibodies used in this study were: anti-clathrin heavy chain (CLH) mouse antiserum [28], 1:2000 dilution; anti-protein disulfide isomerase 2 (PDI2) mouse antiserum, 1:1000 dilution; Cy3-conjugated anti-cyst wall protein 1 (CWP1) mouse monoclonal antibody (Waterborne, New Orleans, LA), 1:60 dilution; Alexa488-conjugated anti-HA mouse monoclonal antibody (Roche Diagnostics GmbH, Manheim, Germany) 1:30 dilution. Fluorophore-conjugated secondary antibodies were purchased from Invitrogen (Basel, Switzerland.) and used at 1: 200 dilution. Microscopy analyses were performed on a Leica DM IRBE fluorescence microscope or on a Leica SP2 AOBS confocal laser-scanning microscope (Leica Microsystems, Wetzlar, Germany), using the appropriate settings. Image stacks of optical sections were further processed using the Huygens deconvolution software package version 2.7 (Scientific Volume Imaging, Hilversum, NL). Three-dimensional reconstruction and surface rendering was done with the Imaris software suite (Bitplane, Zurich, Switzerland) using the surpass functions.

Electron microscopy analysis. Parasite were treated with PPMP or solvent for 16 h and collected as described. The cells were resuspended in 2.5 % glutaraldehyde in 0.1M Na/K-phosphate, pH 7.4, and centrifuged at 3500g for 20 min. After washing, pellets were then postfixed with 1% osmium tetroxide in 0.1M Na/K-phosphate for 1 h, dehydrated in a graded ethanol series,

transferred to acetone for embedding in epon, and polymerized at 60°C for 2.5 days. Ultrathin sections were stained with uranyl acetate and lead citrate and examined at an acceleration voltage of 100 kV in a Philips CM 12 transmission electron microscope (Eindhoven, The Netherlands) equipped with a low scan CCD camera (Gatan, Pleasanton, USA).

Determination of protein concentration. Protein content was determined using the Bio-Rad Protein Assay according to the instructions provided by the manufacturer. Bovine serum albumin was used for the standard curve.

Results

PPMP inhibits glucosylceramide synthesis and increases ceramide levels in G. lamblia. In mammalian cells, PPMP blocks the synthesis of GlcCer by occupying the catalytic site of GCS, the enzyme which transfers one glucose molecule to ceramide. PPMP treatment results in decreased cellular levels of GlcCer and accumulation of the ceramide precursor [29]. To determine whether *G. lamblia* is capable of GlcCer synthesis and whether PPMP inhibits GlcCer formation in the parasite, we metabolically labeled *G. lamblia* trophozoites and analyzed the extracted lipids by two dimensional thin layer chromatography (2D TLC). Labeling with the [^{3}H]palmitic acid precursor showed that 10 μM PPMP, a concentration we previously showed to inhibit *G. lamblia* replication [6], strongly altered the lipid profile by either decreasing (Fig. 1A, spots A, B) or increasing (spots C, D) the abundance of labeled lipids or inducing the appearance of labeled species not visible in the untreated sample (spot E). Saponification of extracted lipids by mild alkaline hydrolysis to remove glycerol-based lipids revealed that lipid "A" was resistant to the treatment, and thus supporting that it belongs to the sphingolipid class (Fig 1B). In addition, 1D TLC of saponified samples showed that the predominant band co-migrated with a GlcCer standard and its amount decreased upon PPMP treatment (Fig 1C), supporting the notion that lipid "A" is GlcCer. To further confirm that the lipid "A" is indeed GlcCer, the spot was cut from the TLC and tested for sensitivity to ceramide glycanase, which hydrolyzes the glucose moiety from glycosphingolipids. While the hydrolysis was not complete, TLC separation revealed a band co-migrating with ceramide in the glycanase treated sample (Fig. 1D), indicating that the lipid in spot "A" is a substrate for the enzyme. In addition, having confirmed that PPMP treatment decreased the synthesis of GlcCer in *G. lamblia*, we next monitored whether GlcCer synthesis inhibition resulted in increased cellular levels of the precursor ceramide. TLC

separation showed that a band co-migrating with ceramide standard is indeed more abundant in the PPMP treated sample (Fig. 1E).

Similarly to the PPMP-mediated inhibition of *G. lamblia* replication [6], PPMP inhibition of GlcCer synthesis was dose-dependent (Fig. 2A). Importantly, GlcCer synthesis was reduced even in cells only pre-treated with 10 μM PPMP for 30 min before drug removal and metabolic labeling (Fig. 2A, Pre), suggesting that the inhibitory effect is not reversible.

Finally, we quantified the reduction of the total GlcCer cellular pool following PPMP treatment. Mass spectrometry analysis readily identified the presence of GlcCer in the parasite (Fig. S1). PPMP treatment for 4 hrs significantly reduced the amount of less abundant GlcCer species (18:0 and 20:0). Of note, the abundance of GlcCer species containing long fatty acid residues (22:0 and 24:0) did not vary in PPMP treated cells, suggesting a different rate of lipid turnover for different GlcCer pools (Fig. 2B). Overall, our data show that, similarly to mammalian cells, PPMP inhibited GlcCer synthesis resulting in increased cellular levels of ceramide in *G. lamblia*.

Metabolic labeling of G. lamblia sphingolipids. G. lamblia is considered to have a limited capability for *de novo* lipid synthesis [30], and only a few candidate enzymes of the sphingolipid synthetic pathway are annotated in the parasite genome [9]. Thus, it is not known whether the parasite is able to carry out a complete *de novo* synthesis of sphingolipids or if it relies solely on host-derived lipid precursors and/or preformed complex lipids. To determine whether GlcCer in cultured *Giardia* trophozoites derives from *de novo* synthesized ceramide or from remodeling of ceramide taken up from the medium, we metabolically labeled the cells with [^{3}H]serine, a substrate for serine palmitoyl transferase (SPT), the first committing enzyme of sphingolipid synthesis which is also annotated in the giardial genome (Fig. S2). Serine was incorporated in the parasite three times less efficiently than palmitic acid (Fig. S3), and labeled one major and few

minor lipid species, which co-migrated neither with ceramide (Fig. 3A) nor with GlcCer (Fig. 3B). In contrast with [^{3}H]palmitic acid labeling, all serine labeled species were alkali-sensitive, and thus glycerol-based lipids (Fig. 3B). Therefore, under these experimental conditions, serine did not label *G. lamblia* sphingolipids, suggesting that the observed ceramide labeling with [^{3}H]palmitic acid is likely to derive from deacylation/reacylation reactions on a pre-existing ceramide pool.

To further elucidate the modality of sphingolipid synthesis, we performed cell labeling with [^{3}H]glucose. This labeled molecule was only weakly incorporated into the lipid fraction of *G. lamblia*, accounting for 6% of the whole cell associated radioactivity (Fig. 4B). However, a band co-migrating with parasite GlcCer was clearly visible after prolonged TLC exposure (Fig. 3C). Similar to the observations during [^{3}H]palmitic acid labeling, PPMP treatment diminished the labeling of GlcCer and increased the intensity of other labeled species.

G. lamblia GlcCer synthesis is not modulated by other sphingolipid inhibitors but by tunicamycin. While a homolog of the first committing enzyme of sphingolipid synthesis, SPT, is found in *G. lamblia*, the other enzymes in the ceramide biosynthesis pathway have not been annotated in the parasite's genome, suggesting that giardial sphingolipid synthesis is incomplete. We then tested whether known inhibitors of these early steps of sphingolipid synthesis [31] (Fig. S2) can inhibit GlcCer formation in the parasite. To do this we performed lipid metabolic analyses in the presence of compounds interfering with (i) the first committed step of sphingolipid synthesis (20 μM myriocin and 500 μM L-cycloserine), (ii) the synthesis of ceramide (50 μM fumonisin B1), and (iii) an additional inhibitor of GCS, structurally unrelated to PPMP (400 μM NB-DNJ). In addition, we tested 60 μM tunicamycin, an amphipatic analog of UDP-GlcNAc, which was shown to inhibit the synthesis of complex glycosphingolipids in

mammalian cells by blocking sugar import into the Golgi apparatus [32-34]. All inhibitors were used at the highest concentration of the range used to affect mammalian sphingolipid synthesis. Interestingly, of all the sphingolipid inhibitors tested, only PPMP was found to decrease GlcCer (Fig. 3D) and to increase ceramide levels (Fig. 3E), while the other compounds did not alter the synthetic capability of the parasite. On the other hand, tunicamycin treatment was found to increase the GlcCer content without affecting ceramide levels (Fig. 3D, E, S4), suggesting that sphingolipid synthesis in the parasite is sensitive to compounds interfering with cellular sugar transport.

Inhibition of GlcCer synthesis promotes lipid turnover. Our previous experiments using tritiated palmitic acid and glucose showed that PPMP increased the labeling of several lipid species different from GlcCer. Such an increase was further quantified by liquid scintillation analysis of the incorporated radioactivity. [^{3}H]palmitic acid incorporation increased both in whole cells and in the lipid fraction of PPMP treated parasites compared with control cells (Fig. 4A), suggesting that the increased lipid incorporation is accompanied by an increased precursor uptake. Interestingly, [^{3}H]glucose incorporation increased in the lipid fraction but not in whole cell extracts (Fig. 4A). To test whether palmitic acid and glucose were differently metabolized into lipids, we quantified the percentage of whole cell-associated precursors found in the lipid fraction. The majority (80-90%) of the cell-associated [^{3}H]palmitic acid was identified in the lipid fraction also after PPMP treatment. Conversely, only 6% of the cell-associated [^{3}H]glucose was found in the lipid fraction, confirming the limited glucose incorporation reported by [11]. However, the amount of lipid-associated glucose increased by 70% in presence of PPMP, suggesting that the intracellular glucose pool is relocated toward a lipid synthetic use (Fig. 4B).

The previously described inhibitors (Fig. 3D, E) were similarly tested in their capability to modulate [^{3}H] palmitic acid incorporation in *G. lamblia* extracts. Consistent with the demonstrated absence of sphingolipid synthesis inhibition, none of the sphingolipid inhibitors altered the incorporation of the labeled precursor into both whole cells and lipids (Fig. 4C).

To identify other lipid classes whose synthesis may be modulated upon PPMP inhibition of GlcCer synthesis, we analyzed the pattern of neutral lipids labeled with [^{3}H]palmitic acid. While 1,2 and 1,3 diacylglycerols (DAG) were the main species present in untreated cells, PPMP treatment dramatically changed the proportion of these lipids, increasing 1,2 DAG levels and reducing 1,3 DAG (Fig. 4D a, b). The observed alteration of neutral lipid synthesis may have been triggered by reduced GlcCer synthesis or increased ceramide levels in PPMP treated cells. To discriminate between these possibilities we increased ceramide levels using cell-permeable C6 ceramide. In these experimental conditions we observed an increase in both 1,2 DAG content (Fig. 4D a, b) and 1,2 and 1,3 DAG ratio (Fig. 4D c), indicating that increased ceramide levels contribute to the observed modulation of neutral lipids.

Increased ceramide levels inhibit G. lamblia cell division. In our previous work, we showed that micromolar concentrations of PPMP arrested parasite cytokinesis and induced the accumulation of partially divided cells in the culture [6]. To directly correlate the replication inhibition with the alteration of sphingolipid synthesis induced by PPMP, we raised the ceramide levels in *G. lamblia* using cell-permeable C6 ceramide, thus mimicking PPMP-induced ceramide increase. Incubation with micromolar concentrations of exogenous C6 ceramide severely inhibited *G. lamblia* replication in a dose-dependent manner, with 30 μM completely arresting parasite division (Fig. 5A, white bars). Importantly, the concomitant presence of PPMP further inhibited parasite replication, indicating that ceramide and PPMP act as agonists on a cellular process

which is involved in parasite replication (Fig. 5A, gray and black bars). Furthermore, quantitative analysis of C6 ceramide treated parasites revealed that exogenous ceramide induced a cytokinesis arrest and accumulation of partially divided cells comparable to the one observed during PPMP treatment (Fig. 5B), indicating that increased ceramide levels are sufficient to inhibit *G. lamblia* cell division.

Similar to the observations described in the lipid analyses above, PPMP was unique amongst the sphingolipid inhibitors tested in both blocking parasite replication (Fig. 5C) and increasing the amount of partially divided cells (Fig. 5D), while the other inhibitors did not affect neither sphingolipid synthesis (Fig. 3D, E) nor parasite cell division (Fig. 5C, D). Furthermore, tunicamycin treatment, which increased cellular GlcCer levels, did not alter parasite replication and doublet formation, suggesting that increased GlcCer levels alone are not sufficient to promote cell division.

In addition, we investigated the effect of PPMP on cell division in more detail and found that the inhibitor exerted a long term block of *G. lamblia* replication after its removal from the culture medium. Parasites treated with the inhibitor for 16 h could not resume cell division even 4 days after PPMP removal, whereas control cells reached the density plateau at day 3 (Fig. 5E). The plasma membrane of treated parasites was visualized with FITC-conjugated cholera toxin (CTX), which binds to the raft-associated sphingolipid GM1 [35]. CTX staining revealed that cytokinesis-arrested parasites had properly formed ventral disks (Fig. 5F, arrowheads) but the cleavage furrow was mainly absent or, in a minority of cases, incomplete (Fig. 5F, arrows).

Ultrastructural abnormalities following inhibition of GlcCer synthesis. To examine the ultrastructure of *G. lamblia* upon inhibition of GlcCer synthesis, we compared control cells with PPMP treated parasites by thin-section transmission electron microscopy. Consistent with our

previous light microscopy observations, we observed an accumulation of partially divided cells in the PPMP-treated samples. In addition, in comparison with untreated cells (Fig. 6E), vesicles bounded by single lipid bilayer membranes accumulated within the cytosol of PPMP-treated parasites (Fig. 6A, arrows and magnified images). Such vesicles had a size of 60-100 nm and a non homogeneous electron-density different from the one observed in peripheral vesicles (PVs). The vesicles were present as clusters beneath the plasma membrane in close proximity with the PVs, juxtaposed to the nuclear envelope, or in the cell interior. PPMP-treated parasites also contained conspicuous electron-lucent vacuoles of various diameters (Fig. 6A, B, C, arrowheads), often located at the posterior end of the parasites. In addition, several vacuoles containing parasite flagella were observed (Fig. 6C asterisks), which have been reported to occur in *G. lamblia* [36] and other anaerobic protists [37] under stress conditions.

Finally, PVs looked generally more distended in PPMP-treated cells (Fig. 6D) and coiled multilamellar structures were also observed, although infrequently (Fig. S5). No gross alterations of parasite morphology such as membrane blebbing, ventral disk fragmentation, electron dense deposits were observed following PPMP treatment.

Inhibition of GlcCer synthesis perturbs clathrin localization and endo-lysosomal compartments, but does not inhibit membrane endocytosis. We hypothesize that vesicle accumulation detected in *G. lamblia* by electron microscopy may result from altered vesicular trafficking as a consequence of exposure to the drug. This hypothesis prompted us to investigate whether PPMP treatment affected the morphology of organelles involved in intracellular trafficking processes. Firstly, we visualized the parasite clathrin (CLH) which is found closely associated with PVs [28], the endo-lysosome system of the parasite [28, 38]. In control cells, the anti-CLH antibody stained punctate structures which were uniformly distributed on the dorsal side of the parasite

and clustered in selected areas on the ventral side, including the area at the centre of the ventral disk (arrow), a signature site for endocytosis [39] (Fig. 7A). PPMP treatment significantly altered the staining pattern and induced aggregation of the punctate structures in the form of elongated or circular clusters.

Next, we monitored the cellular distribution of acidic compartments including PVs in living cells after incubation with lysotracker™ (Fig. 7B). While lysotracker-positive punctate structures of homogeneous size were clearly visible in control cells and were concentrated in the area at the centre of the ventral disk (arrow), in PPMP-treated samples this characteristic pattern was not observed (dashed arrow). Instead, large structures often located at the posterior side of the cell were labeled (arrowhead), most likely corresponding to the large vacuoles observed by transmission electron microscopy analysis.

We then analyzed whether the altered distribution of CLH and lysotracker-positive structures observed upon PPMP treatment were linked to changes in the parasite's ability for endocytosis. To this end, we monitored the internalization of cholera toxin (CTX) bound to the plasma membrane of trophozoites. In mammalian cells, CTX binds to the raft-associated sphingolipid GM1 and enters the cell by retrograde transport in the endocytic pathway [35]. At 4˚C, CTX equally labeled the plasma membrane of both control parasites and parasites treated with PPMP for 30 min or 16 h, suggesting that the inhibitor did not alter GM1 presence on the plasma membrane at the concentration and incubation time used here (Fig. 7C). Following incubation at 37˚C, CTX was internalized showing a punctate pattern reminiscent of PVs. In particular, CTX stained the isolated area at the centre of the ventral disk in a time-dependent manner (Fig. 7C, arrow). Importantly, enumeration of cells showing this endocytosis signature site revealed that CTX was endocytosed in cells treated with PPMP for 30 min (Fig. 7D, a) or 16 h (Fig. 7D, b)

with a kinetic similar to control cells. In addition, mimicking a PPMP–mediated ceramide increase with exogenous C6 ceramide did not compromise CTX endocytosis (data not shown). Collectively, our data indicate that PPMP incubation profoundly modified the cellular organization of CLH and lysotracker positive acidic compartments, suggesting functional alteration of PVs. However, neither drug treatment nor exogenous ceramide inhibited endocytosis of membrane-bound CTX, which is consistant with a principal roles of PVs in fluid phase endocytosis [39].

Inhibition of GlcCer synthesis reduces both synthesis and trafficking of encystation specific proteins. We previously reported that PPMP treatment affected stage differentiation of *G. lamblia* by inhibiting cyst formation [6]. Here we analyzed the molecular mechanisms of PPMP-mediated inhibition of parasite differentiation in more detail. Lipid metabolic analyses of parasites induced to encyst for 16 or 24 hours revealed that, similarly to trophozoites, sphingolipid synthesis was perturbed in presence of PPMP and resulted in decreased GlcCer levels (Fig. 8A) and accumulation of ceramide (not shown).

Next, we monitored whether PPMP affects the fate of cyst wall protein 1 (CWP1), a structural protein whose expression, intracellular trafficking and secretion to form the protective cyst wall are key steps during the encystation process. To quantitatively assess the effect of PPMP on induction of CWP1 synthesis in encysting cells *in vitro*, we performed population-wide analysis of protein expression by flow cytometry 16 h post induction of differentiation. Control cells showed an expected substantial increase in CWP1 fluorescence compared with trophozoites indicative of protein expression during encystation (Fig. 8B). Conversely, PPMP treated cells presented only a modest increase in CWP1 fluorescence, indicating that PPMP severely impaired induction of differentiation. Next we tested whether PPMP treatment inhibited not only CWP1

expression, but also altered the protein's intracellular distribution. Immunofluorescence analysis of encysting parasites showed that in control cells the protein was mainly localized in doughnut-shaped encystation-specific vesicles (ESVs) (Fig. 8C). However, in the minor proportion of PPMP-treated cells which showed detectable CWP1 levels, the protein was localized in numerous elongated structures throughout the cell. Dual staining with the ER-resident protein PDI2 revealed that CWP1 positive-structures partially co-localized with the ER. To investigate whether the altered organelle distribution of CWP1 was a specific consequence of PPMP treatment or a general effect resulting from inhibition of parasite replication and CWP1 synthesis, we blocked *G. lamblia* replication with nocodazole [40] and monitored the effect on CWP1 localization. Exposure to 6 μM nocodazole during the first 16 h of the encystation process inhibited not only replication but also CWP1 synthesis at levels comparable with PPMP treatment (Fig. S6). Microscopic analysis showed that nocodazole-treated parasites were morphologically altered, lost their drop-like shape and became round with enlarged nuclei. However, in a minor proportion of cells which showed CWP1 signal, the protein was localized in vesicular structures with typical ESV morphology (Fig. 8D). As in normal conditions at this stage of differentiation, no CWP1 was observed in the ER (data not shown). Collectively, these data suggest that PPMP treatment specifically impaired not only the induction of CWP1 synthesis but also the trafficking of the protein from the ER to the cell surface.

Finally, we tested whether the observed inhibition of *G. lamblia* encystation derived from ceramide accumulation following PPMP treatment. Increasing the cellular levels of this lipid using cell-permeable C6 ceramide potently reduced cyst formation (Fig. 8E), suggesting that inhibition of encystation following PPMP treatment is likely mediated by ceramide build-up in the parasite.

Molecular characterization of G. lamblia GCS. Because PPMP's inhibitory effect is known to occur via targeting and inhibition of GlcCer synthase, and a putative GlcCer synthase (GlGCS) homolog is annotated in the *G. lamblia* genome (GL50803_11642), we then focused on the characterization of the parasite enzyme. A BLAST database search revealed a number of sequence similarities to deduced amino acid sequences of known GCS, and showed a high homology to plant enzymes in terms of amino acid identity, protein length (Fig. 9A, S7) and hydrophobicity profile (data not shown). Sequence analysis and biochemical data indicated that mammalian GCS belongs to the β-glycosyltransferase family 2 and is a Golgi resident type III integral membrane protein with a non cleavable N-terminal signal sequence, which serves as a transmembrane anchor, and a long cytoplasmic domain containing the enzyme active site (rev. in [41]). Sequence alignment with selected GCS members indicated that signature sequences of the family are conserved in *G. lamblia* GCS, including a putative N-terminal transmembrane domain and a long cytosolic domain (Fig. 9A). Importantly, the *G. lamblia* sequence contains the D1, D2, D3 and (Q/R)*XX*RW motifs, which are considered essential for catalytic activity [42]. Like in the case of mammalian GCS, additional hydrophobic regions are located near the C terminus. While various programs for protein secondary structure prediction (*e.g.* TMpred) predict trans-membrane domains in this region of mammalian GCS, no empirical studies have been performed to determine the exact topology of this GCS region [42].

Mammalian GCS is a Golgi resident integral membrane protein [41]. As *G. lamblia* lacks an identifiable Golgi apparatus [28] but produces developmentally regulated organelles (ESVs) with Golgi-like characteristics [21], we then analyzed the localization of GCS in this parasite. To this aim, recombinant GlGCS fused to a C-terminal HA tag was expressed in transgenic parasites.

Immunofluorescence analysis of stable integrants revealed an intracellular punctuated signal reminiscent of ER pattern (Fig. 9B). Co-immunostaining of the ER-resident protein PDI2 confirmed that GlGCS co-localized to PDI2-positive ER structures in encysting trophozoites (Fig. 9B a). Conversely, co-immunostaining of the encystation-specific protein CWP1 revealed absence of co-localization with GlGCS, indicating that the protein is excluded from ESVs (Fig. 9B b,c).

To investigate the nature of the first N-terminal hydrophobic sequence, HA tags were introduced at the N-terminal end either of the full length GlGCS or of a variant lacking the first hydrophobic stretch (aa 3-22). Both reporters showed an equivalent signal and distribution, indicating that, like the mammalian homologue, the parasite protein is not proteolytically processed to remove the first hydrophobic sequence (data not shown). In addition, similar results were obtained with HA tagging of the full length protein at the C- terminus, suggesting that the tag position does not affect the expression or localization of the recombinant protein (not shown).

G. lamblia GCS regulation during encystation. To investigate whether GlGCS is regulated during parasite stage differentiation, we analyzed the levels of GlGCS mRNA in encysting cells at 7 h post induction, the time when RNA transcription of encystation-specific genes peaks [21]. Microarray analysis showed a significant increase of mRNA for the sphingolipid synthesis enzymes GlGCS and serine palmitoyltransferase 2 in encysting cells compared with trophozoites (Fig. 10A). The same RNA samples were also processed for semi-quantitative real time PCR (Fig. 10B). The analysis revealed that GlGCS mRNA was less abundant than actin mRNA in both trophozoites and encysting cells (actin/GCS ratio<1). Consistent with the microarray data, GlGCS mRNA levels increased in encysting cells compared with trophozoites, although the observed two fold up-regulation was of moderate proportions relative to the considerable sixty

fold up-regulation of CWP1 mRNA. Thus, higher concentrations of GlGCS mRNA were detected at 7 hours encystation using two independent methods, suggesting increased GlGCS activity during parasite stage differentiation. However, contrary to a previous report showing GlcCer accumulation within the cysts by lipid immunostaining [9], our metabolic labeling and lipid analysis did not show increased levels of GlcCer during encystation (Fig. 10C). To determine whether the sphingolipid composition differed during parasite stage-conversion, lipids were extracted from trophozoites and encysting cells and compared by liquid chromatography-mass spectrometry (LC-MS). The analysis revealed that GlcCer levels were comparable in the two stages of the parasite; however, the amount of complex glycosphingolipids and in particular of ceramide trihexoside increased considerably in encysting cells (Fig. 10D), revealing that the glycosphingolipid composition of the parasite changed during stage conversion.

Finally, as we showed that both GCS mRNA and complex sphingolipids synthesis are up-regulated during stage conversion, we hypothesized that GCS over-expression would promote parasite encystation. To test this, we assessed encystation efficiency in transgenic parasites harboring extra copies of GCS. The analysis revealed that GCS over-expression increased the production of cysts compared with control parasites (Fig. 10E), suggesting that GCS activity is sufficient to promote the encystation process in this parasite.

Discussion

GCS is a pivotal enzyme in the sphingolipid biosynthetic pathway, acting both as a hub for the synthesis of more complex glycosphingolipids and as a regulator of cellular ceramide levels. In the present study the role of GCS in the cell cycle and stage differentiation of the pathogenic parasite *G. lamblia* was investigated. We found that pharmacological inhibition of GlcCer synthesis increased the cellular levels of ceramide and consequently inhibited cellular proliferation and cytokinesis. In addition, GCS inhibition correlated with intracellular trafficking defects leading to abortive encystation, indicating that GCS plays a crucial role in parasite's differentiation.

GlcCer biosynthesis. In mammalian cells, PPMP blocks the synthesis of GlcCer by occupying the catalytic site of GCS. In this study we characterized the GlcCer synthesis in *G. lamblia* and its inhibition by PPMP, and found that an active GCS homologue is present in the parasite and that sphingolipid synthesis can be targeted by the inhibitor also in this organism. As in mammalian cells, inhibition of giardial GCS reduced GlcCer synthesis and induced ceramide accumulation. In addition, GCS inhibition increased the overall lipid turn-over in the parasite, and, similar to previous observations in mammalian cells [43], increased the synthesis of the neutral lipid DAG. Enhanced neutral lipid synthesis may partially offset the effects on membrane structure caused by a reduced GlcCer formation; alternatively, DAG accumulation may also be the byproduct of increased sphingomyelin synthesis, attempting to lower the levels of ceramide. In support of this hypothesis, exogenously provided ceramide also increased DAG synthesis, suggesting that the altered neutral lipid synthesis is a compensation mechanism for modulating the cellular content of ceramide.

While the synthesis of GlcCer was clearly demonstrated in the parasite by metabolic labeling with radioactive palmitic acid and glucose, the absence of labeled ceramide when supplying the parasites with [^{3}H]serine supported the notion that the sphingolipid synthetic pathway is incomplete in *G. lamblia* and that the parasite uses host-derived ceramide as a substrate for the synthesis of complex sphingolipids. Thus, similar to remodeling of phospholipids in *Giardia* [18], deacylation/reacylation of preexisting ceramide pools is likely to account for the observed [^{3}H]palmitic acid labeling of ceramide. However, it should be noted that serine incorporation in the parasite was three times less efficient than palmitic acid. This reduced efficiency, combined with the fact that serine is preferentially incorporated into glycerol-based lipids rather than sphingolipids in mammalian cells [44], might be a limiting factor in visualizing sphingolipids in *G. lamblia*. Hence, additional labeled precursors should be used to elucidate the lipid synthetic steps which are active in the parasite. Intriguingly, while a ceramide synthase is not annotated in the *G. lamblia* genome database, the predicted gene product of GL50803_5939 contains a TLC [TRAM/Lag1p/CLN8 (ceroid-lipofuscinoses, neuronal 8)] homology domain (SMART accession no. SM00724), which is typical of the Lass (longevity-assurance homologue) family members. Lass proteins, homologues to the yeast Lag1p/Lac1p, are highly conserved among eukaryotes and function in ceramide synthesis (recently reviewed in [45]). Thus, this *G. lamblia* protein is worthy of careful characterization to elucidate whether a ceramide synthase activity is indeed present in the parasite.

Our metabolic analyses showed that of all the sphingolipid inhibitors tested, PPMP was the only compound able to inhibit GlcCer synthesis in *G. lamblia*. This lack of effect of other sphingolipid inhibitors on *G. lamblia* lipid synthesis can be explained by (i) highly divergent parasite enzymes, not efficiently recognized by the inhibitory compounds; (ii) poor inhibitor

permeability, as described for fumonisin B1 [31], or (iii) incomplete parasite synthetic pathways, lacking the enzymes targeted by the used compounds. Of particular interest is the fact that the imino sugar NB-DNJ, a GCS inhibitor structurally unrelated to PPMP, did not affect GlcCer synthesis in *G. lamblia*. NB-DNJ is a promising compound in mammalian cells, which is able to reduce GlcCer synthesis and is currently used as a substrate reduction therapy drug for treating type I Gaucher disease [46]. However, this inhibitor is not fully specific, as it inhibits β-glycosidase I and II as well as GCS, and is a much less effective inhibitor of GCS *in vitro* than the PDMP class of compounds [42]. In addition, NB-DNJ has been reported to reduce GlcCer levels not only by inhibiting GCS but also by promoting GlcCer catabolism acting as a chemical chaperone of GlcCerase [47]; thus the still undefined presence of this enzyme in the parasite and its efficient targeting by NB-DNJ may be crucial for the GlcCer reduction in *G. lamblia*.

On the other hand, the increased GlcCer synthesis in the parasite following tunicamycin treatment was quite unexpected. In mammalian cells, synthesis of different sphingolipids is compartmentalized, with GlcCer synthesis occurring at the cytosolic face of Golgi membranes and complex sphingolipids at the Golgi lumenal side. *In vivo* and *in vitro* experiments showed that tunicamycin inhibits transport of the nucleotide-sugar UDP-Gal into the Golgi and, as a consequence, synthesis of complex sphingolipids in the Golgi lumenal decreased and the precursor GlcCer accumulated [32-34]. It is not known whether tunicamycin affects nucleotide-sugar transporter activities in *G. lamblia*. However, a single nucleotide-sugar transporter specific for UDP-GlcNAc was recently described in *G. lamblia* and, interestingly, this sugar was preferentially incorporated into glycolipids rather than into proteins [48]. As tunicamycin is a UDP-GlcNAc analog, it is possible that this compound may target the parasite transporter. Thus, the GlcCer accumulation observed in *G. lamblia* following tunicamycin treatment suggests that

sphingolipid synthesis may be compartmentalized also in this parasite. This possibility is quite interesting as such a compartmentalization would be likely to occur not in the Golgi apparatus, which is absent in the parasite [28], but in the ER. In support of this idea, epitope-tagged giardial GCS was localized in the ER and in silico analysis showed a putative cytosolic topology of its active site; thus, it is likely that GlcCer is synthesized on the cytosolic side of the ER and that its translocation to the luminal side may be necessary for further synthesis of complex sphingolipids. In this context, it is worth mentioning that, while mammalian GCS is located in the Golgi apparatus, the Drosophila homologue is also present in ER membranes [49].

Ceramide and cell cycle progression. During the inhibition of GlcCer synthesis, *G. lamblia* progressed through rounds of organelle and DNA replication, but was prevented from completing cytokinesis and forming a cleavage furrow. A possible explanation for the cytokinesis arrest is that inhibition of GlcCer synthesis alters the formation of sphingolipid-rich domains necessary for cytokinesis signaling [50]. However, our results showed that increased ceramide levels alone are sufficient to arrest cytokinesis and to block replication in the parasite, indicating that ceramide has anti-proliferative effects in the parasite. Moreover, the agonistic effect of ceramide and GCS inhibition suggested that GCS acts as a buffer for regulating the amount of bioactive ceramide. In this regard, it is interesting to note that the ER, the location of giardial GCS, is likely to be the place where prompt regulation of ceramide levels take place, as ER structures are indeed the site of ceramide accumulation upon incubation with an exogenous fluorescent analog [15].

Interestingly, a crucial role of GCS in the pathogenesis of a microorganisms was previously decsribed also in the pathogenic fungus *Cryptococcus neoformans,* where GlcCer was found to be a key factor for cell division and virulence [51].

The observed ceramide-mediated inhibitory effects in the parasite following treatment with PPMP, is consistent with anti-proliferative and pro-apoptotic effects of PPMP in mammalian cells after inducing buildup of ceramide [52, 53]. Studies on the existence of a mechanism similar to apoptosis or programmed cell death (PCD) in *G. lamblia* are scarce. Morphological features of PCD following pro-apoptotic drugs, including chromatin condensation, apoptotic bodies and cytoplasmic vacuolation, have been reported; however, our understanding of PCD in *G. lamblia* is limited as the parasite does not harbor bona fide mitochondria, key components in the apoptotic pathways, and typical PCD-mediating proteins, such as caspases, have not been identified in the parasite genome so far [54]. Ceramide is an early mediator of cell cycle arrest and apoptosis, acting upstream of caspase-dependent and independent signaling pathways (recently reviewed in [55]). Interestingly, putative giardial proteins homologues of components of the ceramide signaling cascade, including protein phosphatases PP1, PI3K/AKT and PP2A, [56], are annotated in the *Giardia* genome data base, and the latter was shown to be involved in the differentiation process of the parasite [57]. Thus it is likely that signaling by ceramide, and possibly by other bioactive sphingolipids, is highly conserved also in this simple eukaryote. In support of this hypothesis, we found that psychosine, a sphingolipid which induces cytokinesis arrest [58] and apoptosis [59] in mammalian cells, also inhibited *G. lamblia* cell division at micromolar concentration (our unpublished results). Collectively, our observations suggest that the parasite cell cycle is highly responsive to variations in the cellular levels of bioactive sphingolipids. As the molecular mechanisms of ceramide signaling in eukaryotic cells remains largely undefined due to the high level of complexity, *G. lamblia* with its simple organization and minimized cellular mechanisms [7] can be exploited as a model system to clarify the core components and processes of the signaling machinery.

Vesicular trafficking. Recent studies on a variety of organisms revealed that vesicular trafficking to the cleavage furrow is an essential process for the completion of cytokinesis (rev. in [60]). Our ultrastructural analyses of PPMP-treated samples revealed abnormal accumulations of vesicles, whose diameter resembled that of coated vesicles involved in intracellular trafficking. In addition, the observed enlarged acidic compartments and aberrant clathrin organization implied that defects in intracellular trafficking may occur upon GlcCer synthesis inhibition. Ceramide has been proposed to modulate vesicular trafficking in mammalian cells; however, the characteristics of this modulation differed in various experimental conditions. Similar to the "lysosome phenotype" observed in *Giardia*, increased ceramide levels have been shown to promote the formation of endocytic vesicles and to induce enlarged lysosomes [61]. Enhanced endocytosis after ceramide increase via sphingomyelin degradation was also reported [62]. Conversely, ceramide increase using exogenous ceramide, sphingomyelin degradation or PDMP-mediated GCS inhibition, was shown to compromise fluid-phase endocytosis within minutes and to a lesser extent receptor mediated endocytosis [63]. These divergent phenotypes raise the possibility that ceramide may differentially regulate endocytic processes in different cell types. In our experimental conditions, we found that PPMP treatment altered lysosome morphology and clathrin organization but did not reduce nor enhance internalization of CTX bound to the plasma membrane. It should be noted that the intracellular transport of CTX does not depend on fluid-phase endocytosis; instead it requires raft association and involves both clathrin-dependent and independent mechanism of endocytosis (rev. in [35]). Thus, it is possible that CTX endocytosis in *G. lamblia* occurs via a modality not sensitive to ceramide. However, in light of the fact that fluid phase and receptor mediated endocytosis are differently regulated in the parasite [39], we

cannot exclude that intracellular ceramide levels do not modulate other *G. lamblia* endocytic processes.

Anterograde trafficking of giardial CWP1, a soluble protein which is synthesized during stage differentiation and sorted at the level of ER into encystation specific vesicles [28], was clearly impaired in presence of PPMP, with consequent reduction of CWP1 deposition on the parasite surface and cyst formation. Importantly, treatment with cell permeable C6 ceramide also reduced cyst formation, suggesting that increased levels of cytosolic ceramide are sufficient to inhibit the encystation process in *G. lamblia*.

Studies in mammalian cells more consistently show that raised ceramide levels inhibit anterograde trafficking [64-67], suggesting that intracellular ceramide concentration may serve as a general modulator of anterograde membrane trafficking events. While it is possible that increased ceramide levels in the parasite following GCS inhibition compromise CWP1 trafficking, it is also conceivable that the reduced concentration of GlcCer plays a role in the observed inhibition, as suggested by the increased cyst formation observed during GCS over-expression. Indeed, glycosphingolipids, most likely GlcCer, are required for the vesicular pathway from the Golgi complex to the melanosome (rev. in [68]) . The proposed mechanism is that GlcCer on the cytosolic side of Golgi membrane is required for the formation of a functional protein coat and subsequent vesicle budding. Thus it is tempting to speculate that in *G. lamblia* GlcCer synthesized by ER-resident GCS may contribute to anterograde protein trafficking by either forming membrane microdomains required for sorting of cargo proteins or binding to cytosolic proteins which are necessary for recruiting coat proteins and vesicle budding.

In summary, we have found several novel aspects of sphingolipid metabolism and regulation in *G. lamblia*. Our work revealed that GlcCer synthesis plays a key role in different essential

processes associated with the parasite cell cycle and stage differentiation. In addition, we also showed that inhibition of GCS blocks parasite cell division, which, together with the likely pharmacological discrimination due to low level of giardial GCS identity with the mammalian counterparts, validates the potential of this enzyme as a target for drug development.

Lastly, the presence of an active GCS and the high responsiveness to ceramide in this divergent parasite support the hypothesis that GlcCer synthesis and bioactive sphingolipids have conserved functions in the regulation of eukaryotic cells processes. In this context, the simple cellular system of *G. lamblia* offers a new perspective from which to explore in details the mechanisms of sphingolipid functions and signaling.

Acknowledgments

We thank Norman Radin for invaluable advice and discussion and Therese Michel and Eva Dalmau for technical assistance.

The *Giardia lamblia* microarrays (version 1) were kindly offered through NIAID's Pathogen Functional Genomics Resource Center, managed and funded by Division of Microbiology and Infectious Diseases, NIAID, NIH, DHHS and operated by the J. Craig Venter Institute. The Functional Genomics Centre Zurich, Switzerland (www.fgcz.uzh.ch) is a joint facility of the ETHZH and the University of Zurich. This work was supported by grants of the Marie Heim-Vögtlin Foundation and the Fondation Pierre Mercier pour la Science, Switzerland to SS, grant No. 112327 from the Swiss National Science Foundation to ABH and fellowships from the Stiftung für Forschungsföderung of the University of Zurich, the Roche Research Foundation and Novartis Stiftung für Medizin-Biologische Forschung to CS.

References

(1) Bartke, N. & Hannun, Y. A. 2009. Bioactive sphingolipids: metabolism and function, *J Lipid Res.* **50 Suppl,** S91-6.

(2) Liu, Y. Y., Han, T. Y., Giuliano, A. E. & Cabot, M. C. 2001. Ceramide glycosylation potentiates cellular multidrug resistance, *Faseb J.* **15**, 719-30.

(3) Lucci, A., Cho, W. I., Han, T. Y., Giuliano, A. E., Morton, D. L. & Cabot, M. C. 1998. Glucosylceramide: a marker for multiple-drug resistant cancers, *Anticancer Res.* **18**, 475-80.

(4) Liu, Y. Y., Han, T. Y., Yu, J. Y., Bitterman, A., Le, A., Giuliano, A. E. & Cabot, M. C. 2004. Oligonucleotides blocking glucosylceramide synthase expression selectively reverse drug resistance in cancer cells, *J Lipid Res.* **45**, 933-40.

(5) Bleicher, R. J. & Cabot, M. C. 2002. Glucosylceramide synthase and apoptosis, *Biochim Biophys Acta.* **1585**, 172-8.

(6) Sonda, S., Stefanic, S. & Hehl, A. B. 2008. A sphingolipid inhibitor induces a cytokinesis arrest and blocks stage differentiation in Giardia lamblia, *Antimicrob Agents Chemother.* **52**, 563-9.

(7) Morrison, H. G., McArthur, A. G., Gillin, F. D., Aley, S. B., Adam, R. D., Olsen, G. J., Best, A. A., Cande, W. Z., Chen, F., Cipriano, M. J., Davids, B. J., Dawson, S. C., Elmendorf, H. G., Hehl, A. B., Holder, M. E., Huse, S. M., Kim, U. U., Lasek-Nesselquist, E., Manning, G., Nigam, A., Nixon, J. E., Palm, D., Passamaneck, N. E., Prabhu, A., Reich, C. I., Reiner, D. S., Samuelson, J., Svard, S. G. & Sogin, M. L. 2007.

Genomic minimalism in the early diverging intestinal parasite Giardia lamblia, *Science.* **317**, 1921-6.

(8) Savioli, L., Smith, H. & Thompson, A. 2006. Giardia and Cryptosporidium join the 'Neglected Diseases Initiative', *Trends Parasitol.* **22**, 203-8.

(9) Hernandez, Y., Shpak, M., Duarte, T. T., Mendez, T. L., Maldonado, R. A., Roychowdhury, S., Rodrigues, M. L. & Das, S. 2008. Novel role of sphingolipid synthesis genes in regulating giardial encystation, *Infect Immun.* **76**, 2939-49.

(10) Mattjus, P. 2009. Glycolipid transfer proteins and membrane interaction, *Biochim Biophys Acta.* **1788**, 267-72.

(11) Jarroll, E. L., Muller, P. J., Meyer, E. A. & Morse, S. A. 1981. Lipid and carbohydrate metabolism of Giardia lamblia, *Mol Biochem Parasitol.* **2**, 187-96.

(12) Stevens, T. L., Gibson, G. R., Adam, R., Maier, J., Allison-Ennis, M. & Das, S. 1997. Uptake and cellular localization of exogenous lipids by Giardia lamblia, a primitive eukaryote, *Exp Parasitol.* **86**, 133-43.

(13) Blair, R. J. & Weller, P. F. 1987. Uptake and esterification of arachidonic acid by trophozoites of Giardia lamblia, *Mol Biochem Parasitol.* **25**, 11-8.

(14) Gibson, G. R., Ramirez, D., Maier, J., Castillo, C. & Das, S. 1999. Giardia lamblia: incorporation of free and conjugated fatty acids into glycerol-based phospholipids, *Exp Parasitol.* **92**, 1-11.

(15) Hernandez, Y., Castillo, C., Roychowdhury, S., Hehl, A., Aley, S. B. & Das, S. 2007. Clathrin-dependent pathways and the cytoskeleton network are involved in ceramide endocytosis by a parasitic protozoan, Giardia lamblia, *Int J Parasitol.* **37**, 21-32.

(16) Pope-Delatorre, H., Das, S. & Irwin, L. N. 2005. Uptake of [3H]-gangliosides by an intestinal protozoan, Giardia lamblia, *Parasitol Res.* **96**, 102-6.

(17) Ellis, J. E., Wyder, M. A., Jarroll, E. L. & Kaneshiro, E. S. 1996. Changes in lipid composition during in vitro encystation and fatty acid desaturase activity of Giardia lamblia, *Mol Biochem Parasitol.* **81**, 13-25.

(18) Das, S., Castillo, C. & Stevens, T. 2001. Phospholipid remodeling/generation in Giardia: the role of the Lands cycle, *Trends Parasitol.* **17**, 316-9.

(19) Hehl, A. B., Marti, M. & Kohler, P. 2000. Stage-specific expression and targeting of cyst wall protein-green fluorescent protein chimeras in Giardia, *Mol Biol Cell.* **11**, 1789-800.

(20) Gillin, F. D., Boucher, S. E., Rossi, S. S. & Reiner, D. S. 1989. Giardia lamblia: the roles of bile, lactic acid, and pH in the completion of the life cycle in vitro, *Exp Parasitol.* **69**, 164-74.

(21) Stefanic, S., Morf, L., Kulangara, C., Regos, A., Sonda, S., Schraner, E., Spycher, C., Wild, P. & Hehl, A. B. 2009. Neogenesis and maturation of transient Golgi-like cisternae in a simple eukaryote, *J Cell Sci.* **122**, 2846-56.

(22) Jimenez-Garcia, L. F., Zavala, G., Chavez-Munguia, B., Ramos-Godinez Mdel, P., Lopez-Velazquez, G., Segura-Valdez Mde, L., Montanez, C., Hehl, A. B., Arguello-Garcia, R. & Ortega-Pierres, G. 2008. Identification of nucleoli in the early branching protist Giardia duodenalis, *Int J Parasitol.* **38**, 1297-304.

(23) Rehrauer, H., Zoller, S. & Schlapbach, R. 2007. MAGMA: analysis of two-channel microarrays made easy, *Nucleic Acids Res.* **35,** W86-90.

(24) Smith, G. K. 2005. *Limma: linear models for microarray data*, Springer, New York.

(25) Bligh, E. G. & Dyer, W. J. 1959. A rapid method of total lipid extraction and purification, *Can J Med Sci.* **37**, 911-7.

(26) Munoz-Olaya, J. M., Matabosch, X., Bedia, C., Egido-Gabas, M., Casas, J., Llebaria, A., Delgado, A. & Fabrias, G. 2008. Synthesis and biological activity of a novel inhibitor of dihydroceramide desaturase, *ChemMedChem.* **3**, 946-53.

(27) Merrill, A. H., Jr., Sullards, M. C., Allegood, J. C., Kelly, S. & Wang, E. 2005. Sphingolipidomics: high-throughput, structure-specific, and quantitative analysis of sphingolipids by liquid chromatography tandem mass spectrometry, *Methods.* **36**, 207-24.

(28) Marti, M., Li, Y., Schraner, E. M., Wild, P., Kohler, P. & Hehl, A. B. 2003. The secretory apparatus of an ancient eukaryote: protein sorting to separate export pathways occurs before formation of transient Golgi-like compartments, *Mol Biol Cell.* **14**, 1433-47.

(29) Rani, C. S., Abe, A., Chang, Y., Rosenzweig, N., Saltiel, A. R., Radin, N. S. & Shayman, J. A. 1995. Cell cycle arrest induced by an inhibitor of glucosylceramide synthase. Correlation with cyclin-dependent kinases, *J Biol Chem.* **270**, 2859-67.

(30) Das, S., Stevens, T., Castillo, C., Villasenor, A., Arredondo, H. & Reddy, K. 2002. Lipid metabolism in mucous-dwelling amitochondriate protozoa, *Int J Parasitol.* **32**, 655-75.

(31) Delgado, A., Casas, J., Llebaria, A., Abad, J. L. & Fabrias, G. 2006. Inhibitors of sphingolipid metabolism enzymes, *Biochim Biophys Acta.* **1758**, 1957-77.

(32) Guarnaccia, S. P., Shaper, J. H. & Schnaar, R. L. 1983. Tunicamycin inhibits ganglioside biosynthesis in neuronal cells, *Proc Natl Acad Sci U S A.* **80**, 1551-5.

(33) Yusuf, H. K., Pohlentz, G. & Sandhoff, K. 1983. Tunicamycin inhibits ganglioside biosynthesis in rat liver Golgi apparatus by blocking sugar nucleotide transport across the membrane vesicles, *Proc Natl Acad Sci U S A.* **80**, 7075-9.

(34) Burger, K. N., van der Bijl, P. & van Meer, G. 1996. Topology of sphingolipid galactosyltransferases in ER and Golgi: transbilayer movement of monohexosyl sphingolipids is required for higher glycosphingolipid biosynthesis, *J Cell Biol.* **133**, 15-28.

(35) Lencer, W. I. & Saslowsky, D. 2005. Raft trafficking of AB5 subunit bacterial toxins, *Biochim Biophys Acta.* **1746**, 314-21.

(36) Correa, G. & Benchimol, M. 2006. Giardia lamblia behavior under cytochalasins treatment, *Parasitol Res.* **98**, 250-6.

(37) Granger, B. L., Warwood, S. J., Benchimol, M. & De Souza, W. 2000. Transient invagination of flagella by Tritrichomonas foetus, *Parasitol Res.* **86**, 699-709.

(38) Lanfredi-Rangel, A., Attias, M., de Carvalho, T. M., Kattenbach, W. M. & De Souza, W. 1998. The peripheral vesicles of trophozoites of the primitive protozoan Giardia lamblia may correspond to early and late endosomes and to lysosomes, *J Struct Biol.* ***123***, 225-35.

(39) Gaechter, V., Schraner, E., Wild, P. & Hehl, A. B. 2008. The single dynamin family protein in the primitive protozoan Giardia lamblia is essential for stage conversion and endocytic transport, *Traffic.* **9**, 57-71.

(40) Mariante, R. M., Vancini, R. G., Melo, A. L. & Benchimol, M. 2005. Giardia lamblia: evaluation of the in vitro effects of nocodazole and colchicine on trophozoites, *Exp Parasitol.* **110**, 62-72.

(41) Ichikawa, S. & Hirabayashi, Y. 1998. Glucosylceramide synthase and glycosphingolipid synthesis, *Trends Cell Biol.* **8**, 198-202.

(42) Marks, D. L., Dominguez, M., Wu, K. & Pagano, R. E. 2001. Identification of active site residues in glucosylceramide synthase. A nucleotide-binding catalytic motif conserved with processive beta-glycosyltransferases, *J Biol Chem.* **276**, 26492-8.

(43) Radin, N. S. 1994. Rationales for cancer chemotherapy with PDMP, a specific inhibitor of glucosylceramide synthase, *Mol Chem Neuropathol.* **21**, 111-27.

(44) Andrade, C. M., Trindade, V. M., Cardoso, C. C., Ziulkoski, A. L., Trugo, L. C., Guaragna, R. M., Borojevic, R. & Guma, F. C. 2003. Changes of sphingolipid species in the phenotype conversion from myofibroblasts to lipocytes in hepatic stellate cells, *J Cell Biochem.* **88**, 533-44.

(45) Teufel, A., Maass, T., Galle, P. R. & Malik, N. 2009. The longevity assurance homologue of yeast lag1 (Lass) gene family (Review), *Int J Mol Med.* **23**, 135-40.

(46) Cox, T. M. 2005. Substrate reduction therapy for lysosomal storage diseases, *Acta Paediatr Suppl.* **94**, 69-75; discussion 57.

(47) Alfonso, P., Pampin, S., Estrada, J., Rodriguez-Rey, J. C., Giraldo, P., Sancho, J. & Pocovi, M. 2005. Miglustat (NB-DNJ) works as a chaperone for mutated acid beta-glucosidase in cells transfected with several Gaucher disease mutations, *Blood Cells Mol Dis.* **35**, 268-76.

(48) Banerjee, S., Cui, J., Robbins, P. W. & Samuelson, J. 2008. Use of Giardia, which appears to have a single nucleotide-sugar transporter for UDP-GlcNAc, to identify the UDP-Glc transporter of Entamoeba, *Mol Biochem Parasitol.* **159**, 44-53.

(49) Kohyama-Koganeya, A., Sasamura, T., Oshima, E., Suzuki, E., Nishihara, S., Ueda, R. & Hirabayashi, Y. 2004. Drosophila glucosylceramide synthase: a negative regulator of cell death mediated by proapoptotic factors, *J Biol Chem.* **279**, 35995-6002.

(50) Ng, M. M., Chang, F. & Burgess, D. R. 2005. Movement of membrane domains and requirement of membrane signaling molecules for cytokinesis, *Dev Cell.* **9**, 781-90.

(51) Rittershaus, P. C., Kechichian, T. B., Allegood, J. C., Merrill, A. H., Jr., Hennig, M., Luberto, C. & Del Poeta, M. 2006. Glucosylceramide synthase is an essential regulator of pathogenicity of Cryptococcus neoformans, *J Clin Invest.* **116**, 1651-9.

(52) Chan, S. Y., Hilchie, A. L., Brown, M. G., Anderson, R. & Hoskin, D. W. 2007. Apoptosis induced by intracellular ceramide accumulation in MDA-MB-435 breast carcinoma cells is dependent on the generation of reactive oxygen species, *Exp Mol Pathol.* **82**, 1-11.

(53) Litvak, D. A., Bilchik, A. J. & Cabot, M. C. 2003. Modulators of ceramide metabolism sensitize colorectal cancer cells to chemotherapy: a novel treatment strategy, *J Gastrointest Surg.* **7**, 140-8; discussion 148.

(54) Chose, O., Sarde, C. O., Noel, C., Gerbod, D., Jimenez, J. C., Brenner, C., Capron, M., Viscogliosi, E. & Roseto, A. 2003. Cell death in protists without mitochondria, *Ann N Y Acad Sci.* **1010**, 121-5.

(55) Lahiri, S. & Futerman, A. H. 2007. The metabolism and function of sphingolipids and glycosphingolipids, *Cell Mol Life Sci.* **64**, 2270-84.

(56) Ogretmen, B. & Hannun, Y. A. 2004. Biologically active sphingolipids in cancer pathogenesis and treatment, *Nat Rev Cancer.* **4**, 604-16.

(57) Lauwaet, T., Davids, B. J., Torres-Escobar, A., Birkeland, S. R., Cipriano, M. J., Preheim, S. P., Palm, D., Svard, S. G., McArthur, A. G. & Gillin, F. D. 2007. Protein phosphatase 2A plays a crucial role in Giardia lamblia differentiation, *Mol Biochem Parasitol.* **152**, 80-9.

(58) Kozutsumi, Y., Kanazawa, T., Sun, Y., Yamaji, T., Yamamoto, H. & Takematsu, H. 2002. Sphingolipids involved in the induction of multinuclear cell formation, *Biochim Biophys Acta.* **1582**, 138-43.

(59) Giri, S., Khan, M., Rattan, R., Singh, I. & Singh, A. K. 2006. Krabbe disease: psychosine-mediated activation of phospholipase A2 in oligodendrocyte cell death, *J Lipid Res.* **47**, 1478-92.

(60) Albertson, R., Riggs, B. & Sullivan, W. 2005. Membrane traffic: a driving force in cytokinesis, *Trends Cell Biol.* **15**, 92-101.

(61) Li, R., Blanchette-Mackie, E. J. & Ladisch, S. 1999. Induction of endocytic vesicles by exogenous C(6)-ceramide, *J Biol Chem.* **274**, 21121-7.

(62) Zha, X., Pierini, L. M., Leopold, P. L., Skiba, P. J., Tabas, I. & Maxfield, F. R. 1998. Sphingomyelinase treatment induces ATP-independent endocytosis, *J Cell Biol.* **140**, 39-47.

(63) Chen, C. S., Rosenwald, A. G. & Pagano, R. E. 1995. Ceramide as a modulator of endocytosis, *J Biol Chem.* **270**, 13291-7.

(64) Rosenwald, A. G. & Pagano, R. E. 1993. Inhibition of glycoprotein traffic through the secretory pathway by ceramide, *J Biol Chem.* **268**, 4577-9.

(65) Maceyka, M. & Machamer, C. E. 1997. Ceramide accumulation uncovers a cycling pathway for the cis-Golgi network marker, infectious bronchitis virus M protein, *J Cell Biol.* **139**, 1411-8.

(66) Giussani, P., Maceyka, M., Le Stunff, H., Mikami, A., Lepine, S., Wang, E., Kelly, S., Merrill, A. H., Jr., Milstien, S. & Spiegel, S. 2006. Sphingosine-1-phosphate phosphohydrolase regulates endoplasmic reticulum-to-golgi trafficking of ceramide, *Mol Cell Biol.* **26**, 5055-69.

(67) Nakamura, M., Kuroiwa, N., Kono, Y. & Takatsuki, A. 2001. Glucosylceramide synthesis inhibitors block pharmacologically induced dispersal of the Golgi and anterograde membrane flow from the endoplasmic reticulum: implication of sphingolipid metabolism in maintenance of the Golgi architecture and anterograde membrane flow, *Biosci Biotechnol Biochem.* **65**, 1369-78.

(68) van Meer, G., Wolthoorn, J. & Degroote, S. 2003. The fate and function of glycosphingolipid glucosylceramide, *Philos Trans R Soc Lond B Biol Sci.* **358**, 869-73.

Figure Legends

Figure 1: PPMP inhibits GlcCer synthesis in *G. lamblia*. Isolated parasites were labeled with [^{3}H]palmitic acid for 3 h in presence of 10 μM PPMP or solvent (cntl). A. Lipid aliquots corresponding to equal protein amount were separated by 2D-HPTLC using the solvent system A. Note the decreased (spots A, B) or increased (spots C, D, E) abundance of labeled lipids in presence of the inhibitor. B. Saponification of extracted lipids by mild alkaline hydrolysis (NaOH) and separation as described before revealed that lipid "A" belongs to the sphingolipids class. C. Saponified lipid aliquots corresponding to equal protein amount were separated by 1D-HPTLC using the solvent system B. Note the decreased amount of the band co-migrating with a GlcCer standard (GC) upon 10 μM PPMP treatment. D. Spot A was cut from the TLC and hydrolyzed with ceramide glycanase, as described in the Experimental Procedures section. Samples were then separated by 1D-HPTLC using the solvent system B. E. 1D-HPTLC of lipids corresponding to equal protein amount using the solvent system C for ceramide (Cer) separation. Note the ceramide increase upon 10 μM PPMP treatment. O, Ori, origin.

Figure 2: Dose-response inhibition of GlcCer synthesis following PPMP treatment. Isolated parasites were labeled with [^{3}H]palmitic acid for 3 h in presence of solvent (cntl), or PPMP at the indicated concentrations. Alternatively, parasites were pretreated with 10 μM PPMP for 30 min, washed and labeled with [^{3}H]palmitic acid as described before (Pre). Lipid aliquots corresponding to equal protein amount were separated by 1D-

HPTLC using the solvent system B. GlcCer (GC) levels are expressed as percentage of untreated samples (cntl); data are average ± SE (n=3) of a representative from two experiments done in triplicate. B. Liquid chromatography-mass spectrometry analysis of glucosylceramides extracted from trophozoites treated for 4 h with of 10 μM PPMP or solvent (cntl). Data are average ± SE (n=3). *A significant difference (P<0.05) when compared to the percentage of control treated parasites, two-tailed Student's *t*-test.

Figure 3: *G. lamblia* incorporates [^{3}H]glucose but not [^{3}H]serine in GlcCer. A. Isolated parasites were labeled with [^{3}H]palmitic acid (Palm) or [^{3}H]serine (Ser) for 3 h and the extracted lipids separated by 1D-HPTLC using the solvent system C. For serine-labeled samples, lipid aliquots corresponding to three times the protein amount of palmitic acid-labeled samples were used to compensate for the reduced incorporation efficiency. Note the absence of ceramide labeling with serine. B. Extracted lipids were saponified by mild alkaline hydrolysis (NaOH) and separated using the solvent system B. Note the complete hydrolysis of the serine-labeled lipids. C. Parasites were labeled with [^{3}H]glucose in presence of 10 μM PPMP or solvent alone. Extracted lipids were separated using the solvent system B. Note the decreased amount of the band co-migrating with GlcCer upon PPMP treatment. Ori, origin. D. Isolated parasites were labeled with [^{3}H]palmitic acid for 3 h in presence of solvent (cntl), 10 μM PPMP, 50 μM fumonisin B1 (FB1), 20 μM myriocin (Myr), 500 μM L-cycloserine (L-cyc), 400 μM NB-DNJ, and 60 μM tunicamycin (TM). Lipid aliquots corresponding to equal protein amount were separated by 1D-HPTLC using the solvent system B or C (panel E). GlcCer (GC) and ceramide (Cer) levels are expressed as percentage of untreated samples (cntl); data are average ±

SE (n=3) of a representative from three experiments done in triplicate. Note the opposite effect of PPMP and TM treatment on GlcCer levels.

Figure 4: Inhibition of GlcCer synthesis promotes *G. lamblia* lipid turnover. Isolated parasites were labeled with [^{3}H]palmitic acid or [^{3}H]glucose for 3 h in presence of solvent (cntl) or 10 μM PPMP. [^{3}H] incorporation was measured in both whole cell (TOT) and lipid extracts by liquid scintillation and normalized by protein content. A. Incorporation is expressed as percentage of untreated samples (cntl, dashed line); data are average ± SE (n=9) of three experiments done in triplicate. Note that PPMP treatment increased [^{3}H]palmitic acid incorporation both in whole cells and in the lipid fraction, while only in the lipid fraction in the case of [^{3}H]glucose. B. [^{3}H] incorporation in the lipid fraction is expressed as percentage of whole cell-associated precursors. Note the readily incorporation into lipids of [^{3}H]palmitic acid, compared with [^{3}H]glucose and the increased [^{3}H]glucose incorporation upon PPMP treatment. C. Comparison of [^{3}H]palmitic acid incorporation in *G. lamblia* extracts as described in panel A upon treatment with solvent (cntl), 10 μM PPMP, 50 μM fumonisin B1 (FB1), 20 μM myriocin (Myr), 500 μM L-cycloserine (L-cyc), 400 μM NB-DNJ, and 60 μM tunicamycin (TM). Incorporation is expressed as percentage of untreated samples (cntl, dashed line); data are average ± SE (n=9) of three experiments done in triplicate. D. Isolated parasites were labeled with 4 μCi/mL of [^{3}H]palmitic acid for 3 h in presence of solvent (cntl), 10 μM PPMP (PP) or 500 μM C6 ceramide (C6). Lipid aliquots corresponding to equal protein amount were separated using the solvent system D. Part a, representative 1D-HPTLC. DAG, diacylglycerols, Ori, origin. Part b, quantification of lipid levels expressed as percentage of untreated samples (cntl); data are average ± SE

(n=6) of two experiments done in triplicate. Part c, ratio of 1,2 and 1,3 DAG upon C6 ceramide treatment. Data are average ± SE (n=6) of two experiments done in triplicate. Note the increase in 1,2 DAG level in PPMP and C6 ceramide treated samples.

Figure 5: Ceramide modulates *G. lamblia* cell division. A. Freshly inoculated cultures were treated for 16 h with solvent (cntl) or the indicated concentrations of C6 ceramide in absence (white bars) or presence of 5 μM (gray bars) or 10 μM (black bars) PPMP. Parasites were then harvested and counted; cell numbers are expressed as percentage of untreated samples (cntl). Data are average ± SE (n=6) of two experiments done in triplicate. Note the agonistic inhibition of parasite replication of C6 ceramide and PPMP. B. Parasite cultures were treated with the indicated concentrations of C6 ceramide and 10 μM PPMP and incompletely divided parasites (doublets) were counted. Results are presented as percentage of total parasite number (TOT) ± SE (n = 6) of two experiments done in triplicate. Inset: differential interference contrast (DIC) image of a cell doublet. C. Freshly inoculated cultures were treated for 16 h with solvent (cntl), 10 μM PPMP, 50 μM fumonisin B1 (FB1), 20 μM myriocin (Myr), 500 μM L-cycloserine (L-cyc), 400 μM NB-DNJ, and 60 μM tunicamycin (TM). Cell numbers are expressed as percentage of untreated samples (cntl). Data are average ± SE (n=9) of three experiments done in triplicate. D. Parasite cultures were treated as above and incompletely divided parasites (doublets) were counted. Doublet number for FB1-treated cells was not determined. Results are presented as percentage of total parasite number (TOT) ± SE (n = 6) of two experiments done in triplicate. E. Freshly inoculated cultures of trophozoites were treated with 10 μM PPMP or solvent (cntl) for 16 h. After drug removal, parasites were enumerated daily for the following four days. Results of a representative experiment are

presented as average ± SE (n = 6). F. Parasite cultures were treated with 10 μM PPMP for 16 h and the plasma membrane stained with FITC-conjugated cholera toxin (CTX). Note the properly formed ventral disks (arrowheads) and the absent or incomplete cleavage furrow (arrows) in incompletely divided parasites. Nuclear staining was performed with DAPI. Scale bar: 3 μm.

Figure 6: Ultrastructural abnormalities following inhibition of GlcCer synthesis. Electron micrographs of *G. lamblia* treated with 10 μM PPMP for 16 h. Note the cytosolic accumulation of vesicles (A, thick arrows), the electron-lucent vacuoles of various diameters (A, B, C, arrowheads), the presence of vacuoles containing parasite flagella (C, asterisks), and distended peripheral vesicles (D). E. Untreated control parasites. N, nucleus. PV, peripheral vesicles. Scale bar: 3 μm, except in panel D and right part of panel C (0.5 μm).

Figure 7: Inhibition of GlcCer synthesis alters clathrin localization and endo-lysosomal compartments. A. Parasite cultures were treated with solvent (cntl) or 10 μM PPMP for 16 h and stained with anti-clathrin (CLH) antibody. Note the aggregation of CLH-positive punctuated structures upon PPMP treatment. Arrow, signature site for endocytosis. B. Lysotracker™ staining of acidic compartments in parasites treated as in panel A. Note the reduction of the punctuated staining (dashed arrow) and the appearance of large structures (arrowhead) in PPMP-treated cells. Arrow, signature site for endocytosis. C. Parasite cultures were treated with solvent (cntl) or 10 μM PPMP for 16 h and stained with cholera toxin (CTX) at 4ºC to label the plasma membrane. Following a 37˚C incubation, CTX is internalized and labels the endocytosis signature site (arrow) in

both control and drug treated samples. D. Part a, time course of cells treated for 30 min with 10 μM PPMP, stained with CTX at 4ºC and showing the endocytosis signature site following a 37˚C incubation for the indicated time. Part b, cells were treated with 10 μM PPMP for 16 h, labeled with CTX as before and counted for endocytosis signature site-staining after 90 min of 37˚C incubation. Results are presented as percentage of total parasite number ± SE (n = 6) of two experiments done in triplicate. Scale bars: 3 μm.

Figure 8: Inhibition of GlcCer synthesis perturbs CWP1 trafficking. A. Parasites were isolated 24 h post induction of encystation and labeled with [^{3}H]palmitic acid for 3 in presence of 10 μM PPMP or solvent (cntl). Lipid aliquots corresponding to equal protein amount were separated by 2D-HPTLC using the solvent system A. Note the decreased GlcCer levels (spot A) in presence of the inhibitor. B. FACS analysis of parasites encysted for 16 h in presence of solvent (cntl) or 10 μM PPMP and stained for CWP1. Note the modest CWP1 expression in PPMP-treated samples. T, CWP1-stained trophozoites, used as negative control of CWP1 expression. C. Fluorescence analysis of parasites encysted for 16 h in presence of 10 μM PPMP or solvent (cntl) and stained for CWP1 (red), ER-marker PDI1 (green) and nuclei (blue). Upper images, maximum projections; lower images, single optical sections of the deconvolved image stacks. Insets: differential interference contrast (DIC) images. Note the co-localization of CWP1 and PDI2 in PPMP-treated samples. D. Fluorescence analysis of parasites encysted for 16 h in presence of 6 μM nocodazole and stained for CWP1 (red) and nuclei (blue). DIC, differential interference contrast image. Scale bars: 3 μm. E. Parasites were encysted for 16 h in presence of 10 μM PPMP, 20 μM C6 ceramide or solvent (cntl) and stained for

CWP1. Cyst number (out of the total cell number) is presented as percentage of control ± SE (n = 3) of a representative from two experiments done in triplicate.

Figure. 9: Giardial GCS belongs to the β-glycosyltransferase family 2 and localizes into ER. A. Protein sequence alignment of GCS orthologues. Black or gray shading indicates highly conserved amino acids among all the sequences or between *G. lamblia* and plant GCS, respectively. Indicated are the D1,D2,D3,Q/R*XX*RW motifs, which are essential for enzyme activity as demonstrated by site-directed mutagenesis of mammalian GCS. PSORTII predicted transmembrane domains are boxed with solid (strict cutoff) or dashed (loose cutoff) lines. Alignments were performed with Multalin (http://bioinfo.genopole-toulouse.prd.fr/multalin/) and shading was produced with GeneDoc (http://www.psc.edu/biomed/genedoc). B. Fluorescence analysis of parasites expressing recombinant giardial GCS fused to a C-terminal HA tag (green) and encysted for 16 h. Cells were co-stained for ER-marker PDI2 (part a, red), CWP1 (part b, red), and nuclei (blue). Insets: differential interference contrast (DIC) images. Note the GCS co-localization with the ER marker PDI2 and the absence of co-localization with CWP1. Part c, isosurface model of deconvolved confocal image stack showing giardial GCS (green) and CWP1 (red). Scale bars: 3 μm.

Figure 10. Giardial GCS is upregulated during parasite stage conversion. A. Microarray analysis at 7 h encystation showing upregulation of the sphingolipid synthesis enzymes GCS and serine palmitoyltransferase 2 compared with trophozoites. Upregulation of cyst wall proteins is shown as positive control. Gene loci are the following: cyst wall protein 1 (CWP1, GL50803_5638), cyst wall protein 2 (CWP2, GL50803_5435), cyst wall protein

3 (CWP3, GL50803_2421), glucosyceramide synthase (GCS, GL50803_11642), serine palmitoyltransferase 2 (SPT2, GL50803_14374), fatty acid elongase 1 (FAE1, GL50803_92729). B. Semi-quantitative real time PCR indicating the upregulation of GCS and CWP1 at 7 h encystation (EN) compared with trophozoite samples (T). Gene expression levels were given as values in arbitrary units relative to the amount of the constitutively expressed house-keeping gene actin. Data are average ± SE (n = 3) of a representative from two experiments done in triplicate. C. Isolated trophozoites (T) or parasites encysted for 24 h (EN) were labeled with 4 μCi/mL of [^{3}H]palmitic acid for 3 h in supplemented PBS. Lipid aliquots corresponding to equal protein amount were separated by 2D-HPTLC using the solvent systems A. Glucosylceramide (GC) levels were expressed as percentage of trophozoite levels; data are average ± SE (n=3) of a representative from three experiments done in triplicate. D. LC-MS analysis of glycosphingolipids isolated from trophozoites (T) and 24 h encysted cells (EN). GlcCer, glucosylceramide; LacCer, lactosylceramide, GM3 ganglioside (sialic acid, galactosyl-, glucosylceramide), GD3 ganglioside (sialic acid, sialic acid, galactosyl-, glucosylceramide); GGGCer, ceramide trihexoside. Data are average ± SE (n=3) of a representative from two experiments done in triplicate. E. Parasites expressing recombinant giardial GCS or an empty plasmid (cntl) were encysted for 16 h and stained for CWP1. Cyst number is presented as percentage of total cell number (TOT) ± SE (n = 3) of a representative from three experiments done in triplicate.

Figure 1

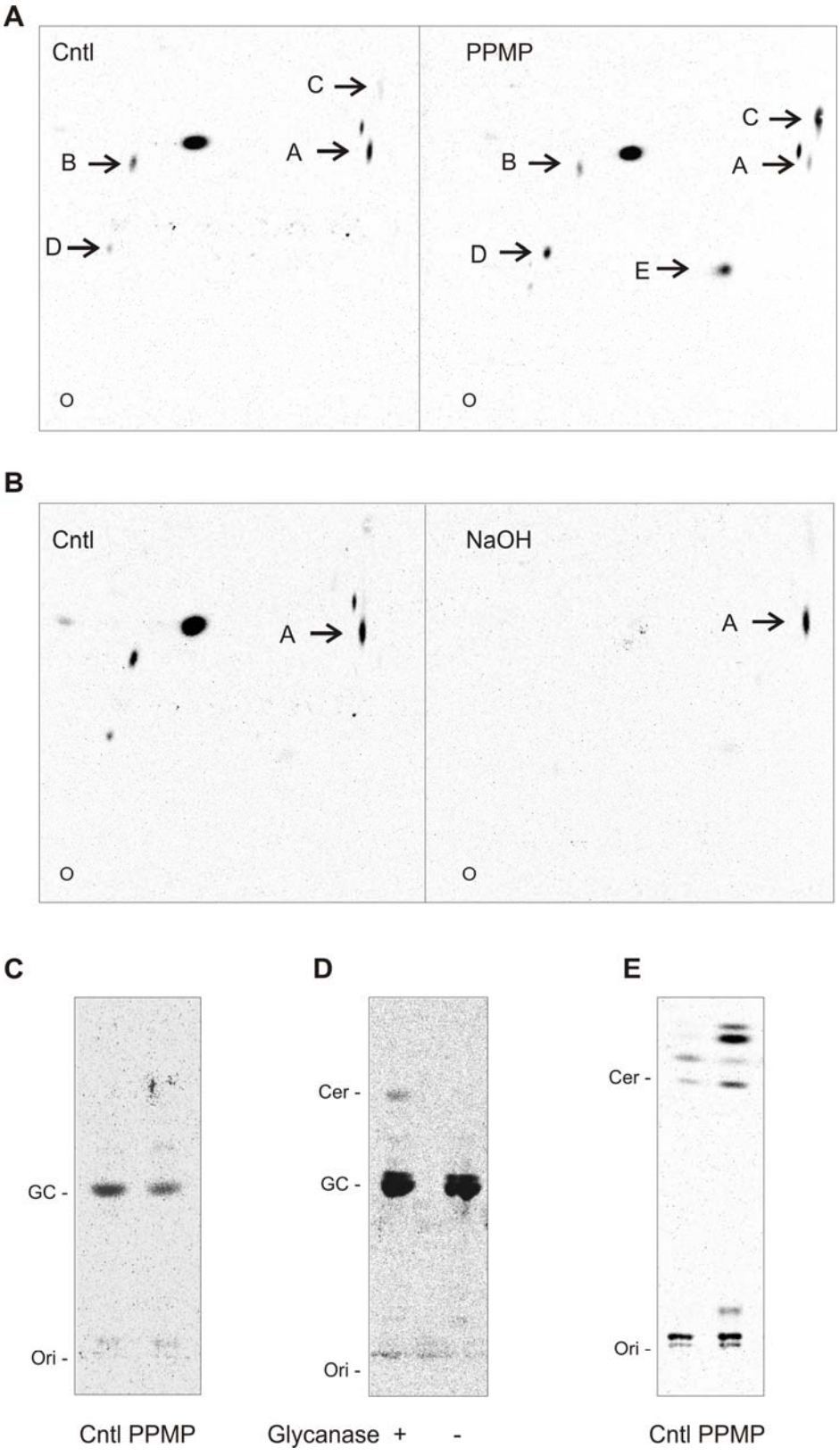

Figure 2

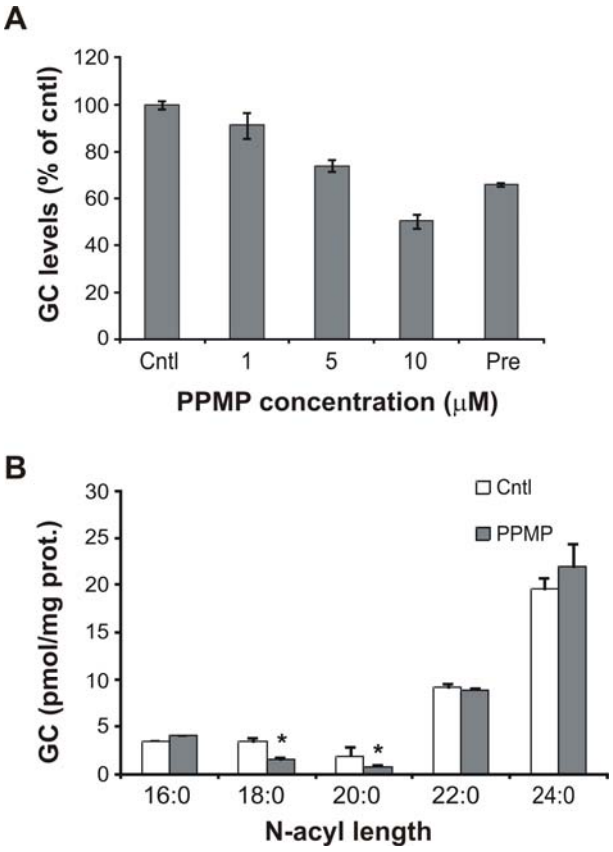

Figure 3

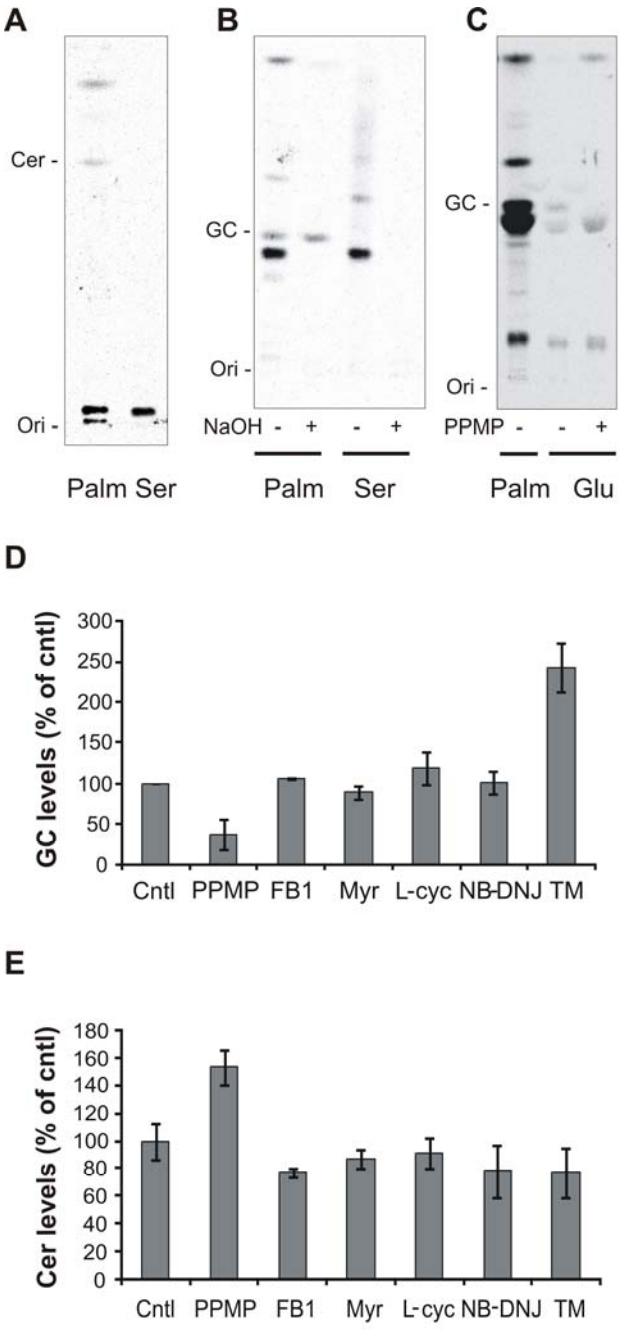

Figure 4

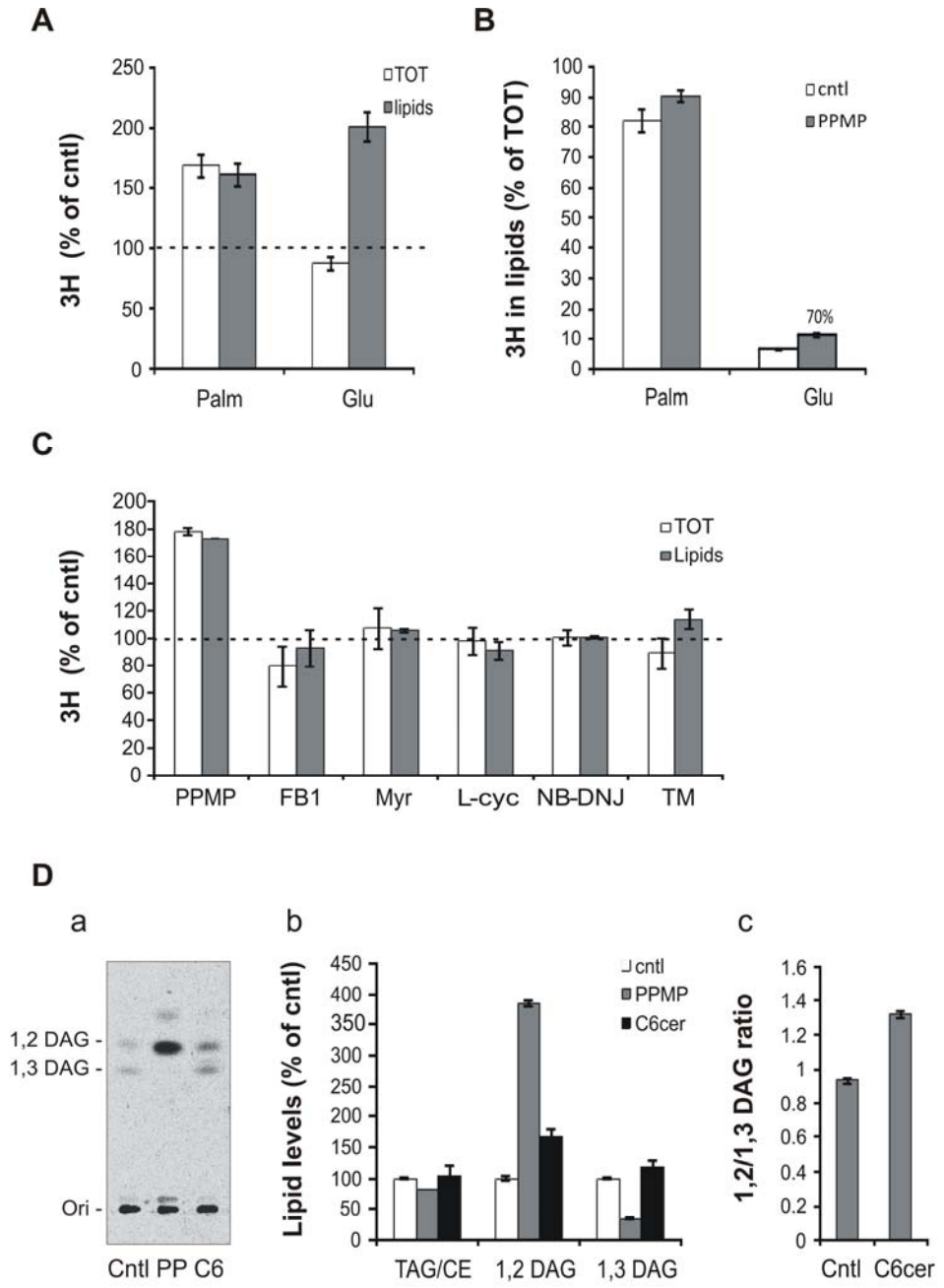

Figure 5

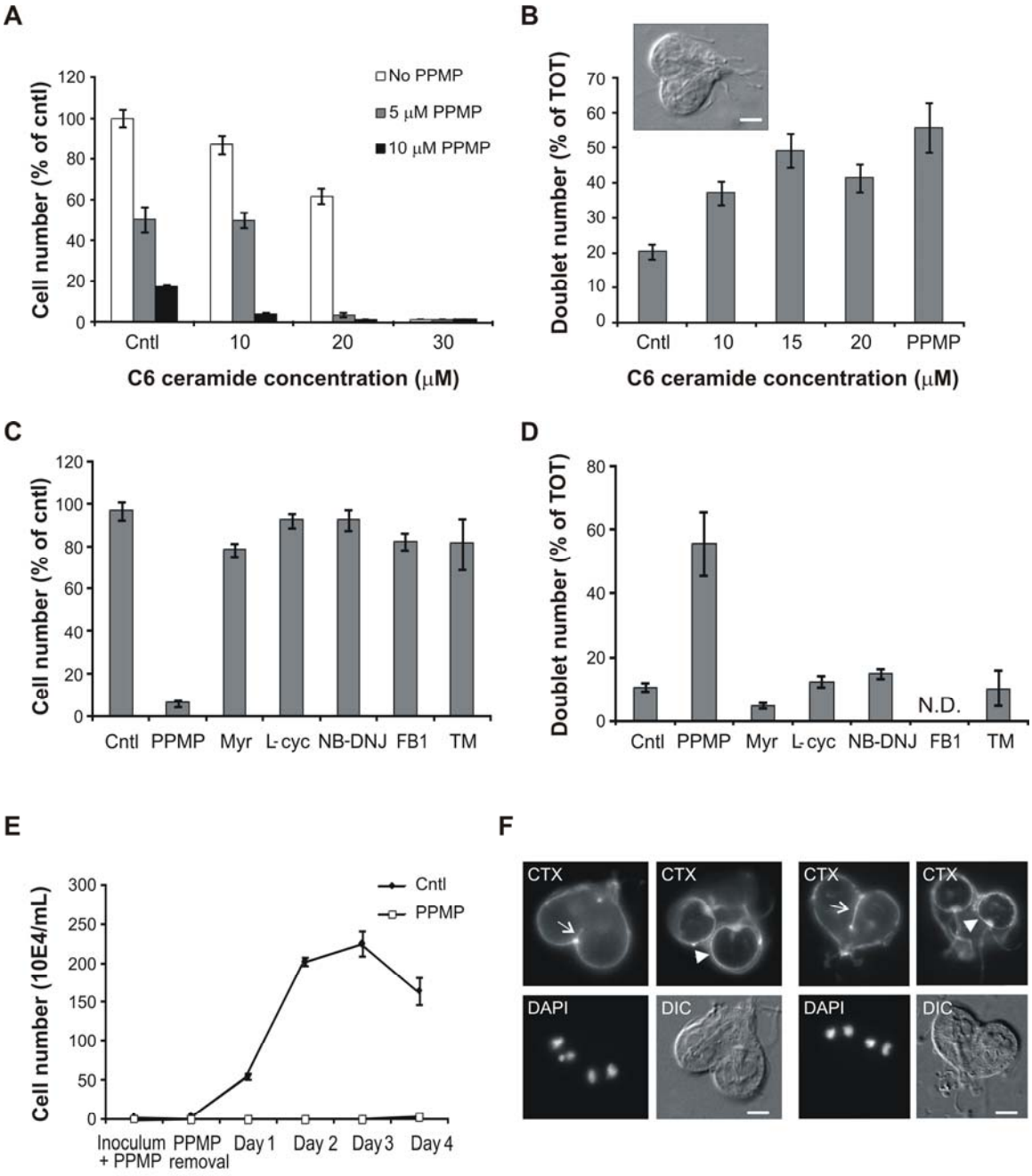

Figure 6

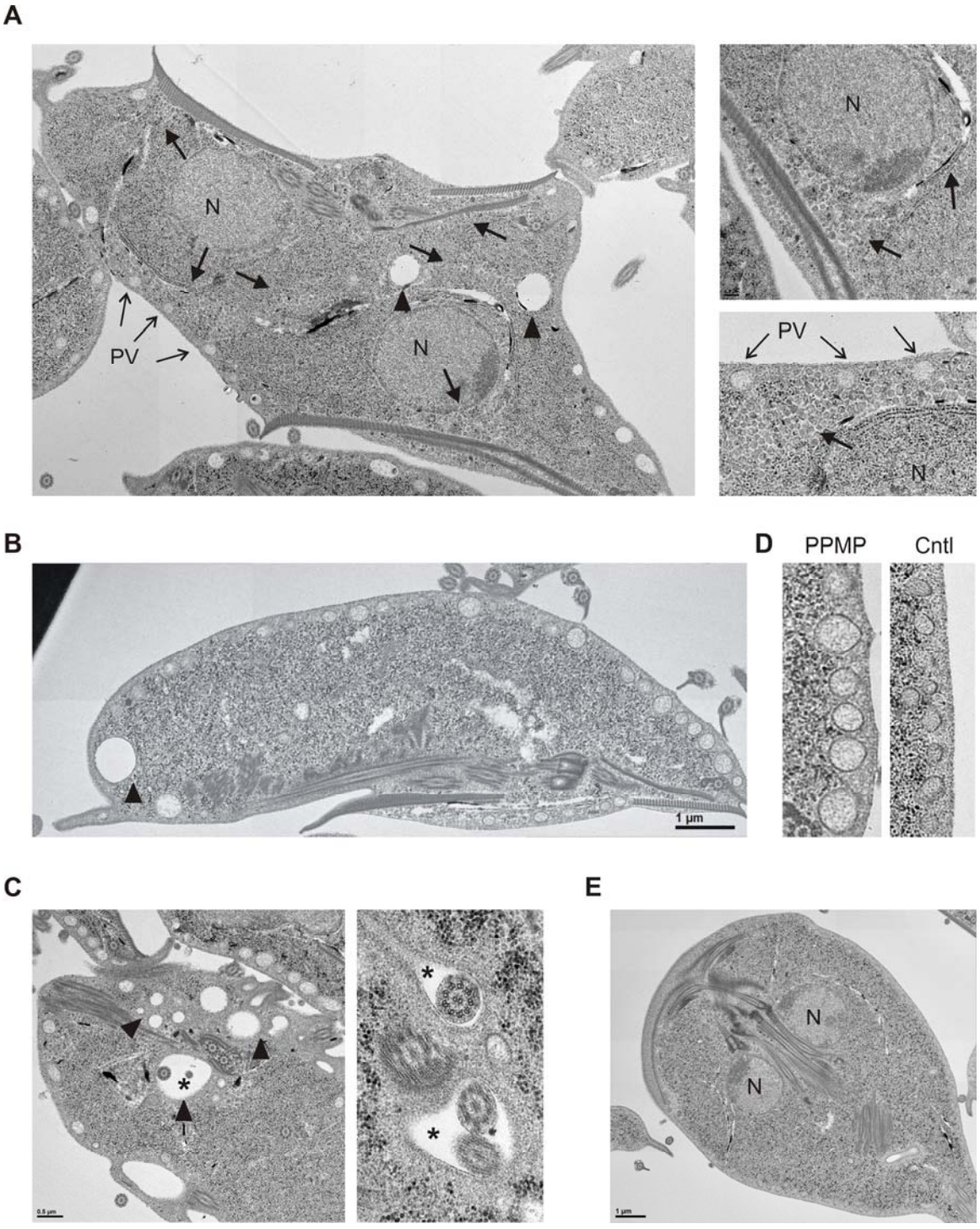

Figure 7

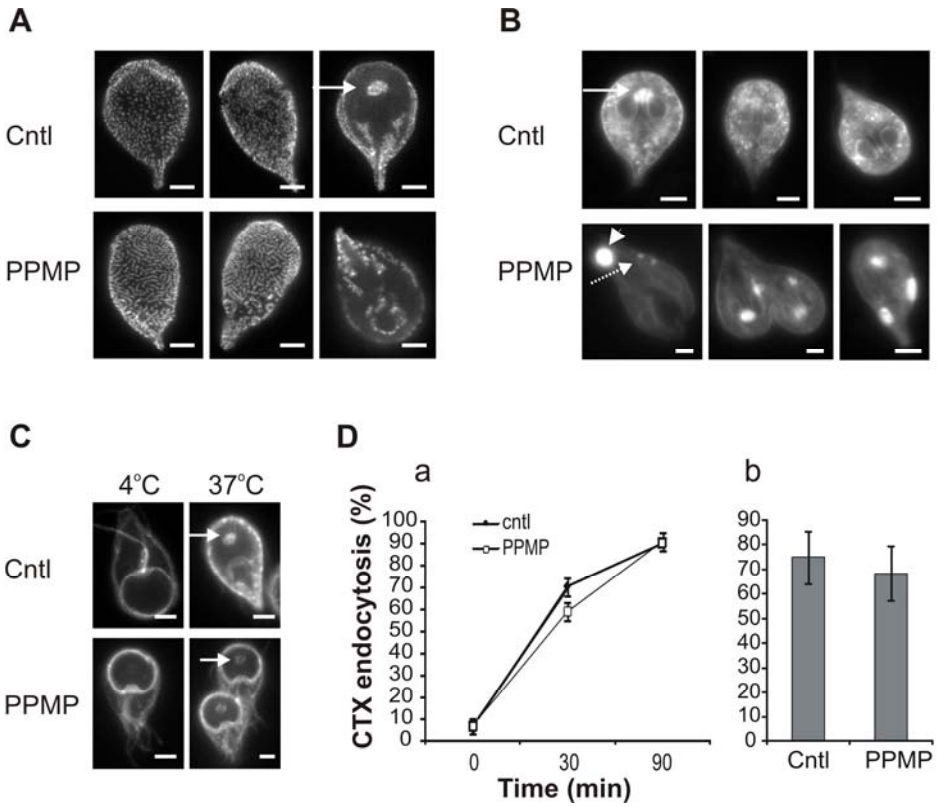

Figure 8

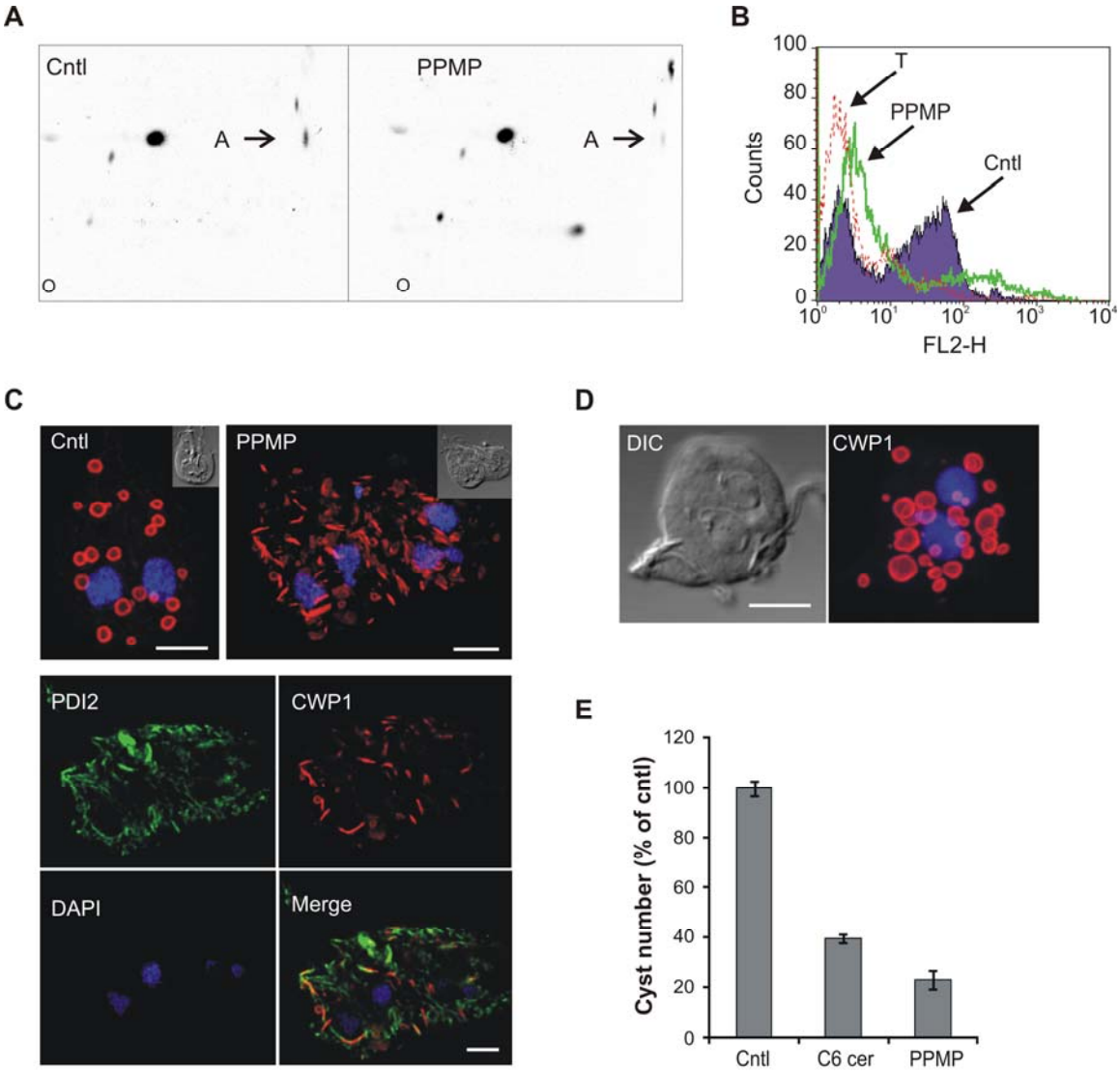

Figure 9

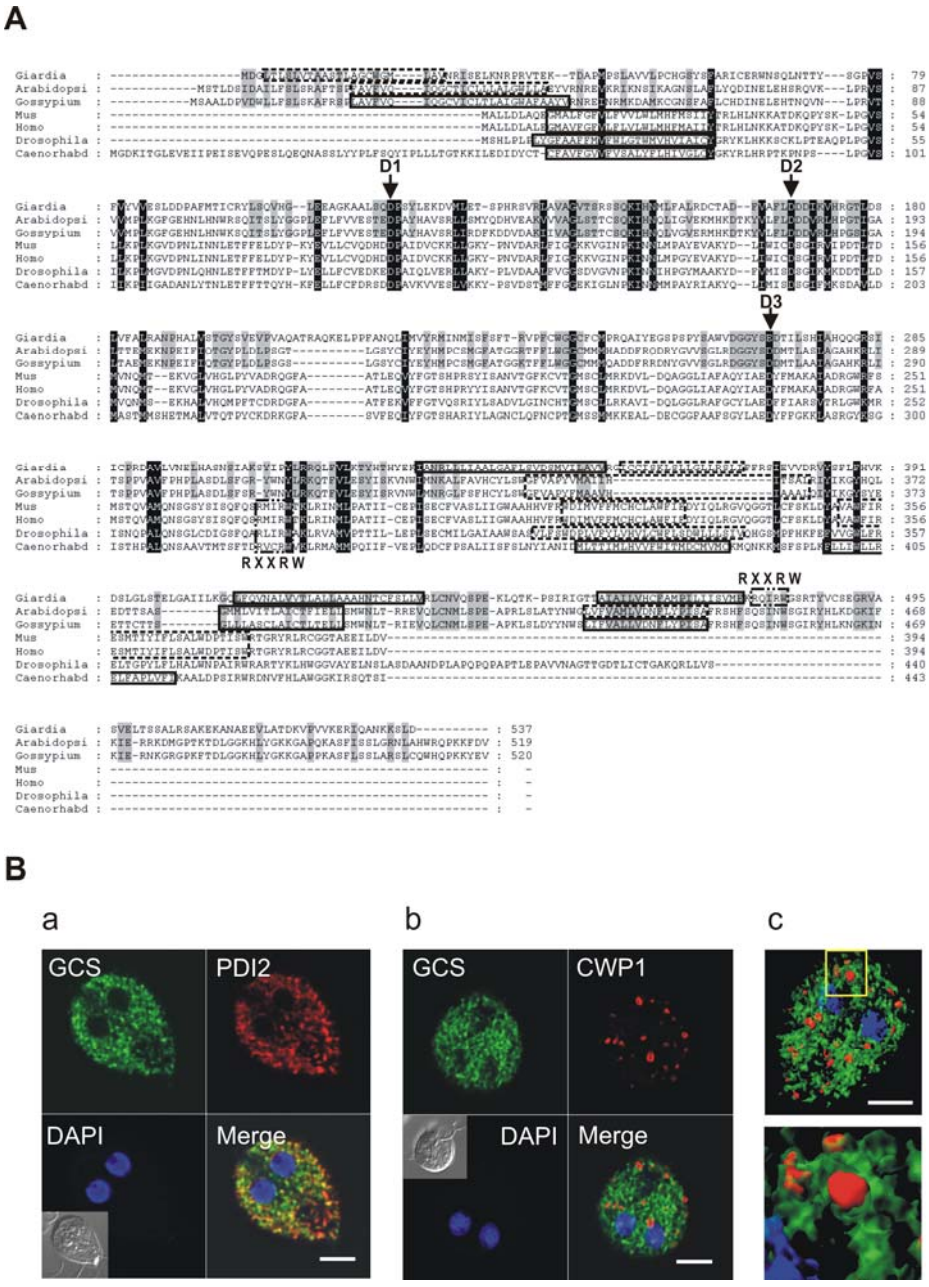

Figure 10